The Influence of Midlatitude Ocean–Atmosphere Coupling on the Low-Frequency Variability of a GCM. Part I: No Tropical SST Forcing*

ILEANA BLADÉ

Joint Institute for the Study of the Atmosphere and Ocean, University of Washington, Seattle, Washington

(Manuscript received 9 July 1996, in final form 5 November 1996)

ABSTRACT

This study examines the extent to which the thermodynamic interactions between the midlatitude atmosphere and the underlying oceanic mixed layer contribute to the low-frequency atmospheric variability. A general circulation model, run under perpetual northern winter conditions, is coupled to a motionless constant-depth mixed layer in midlatitudes, while elsewhere the sea surface temperature (SST) is kept fixed; interannual tropical SST forcing is not included. It is found that coupling does not modify the spatial organization of the variability. The influence of coupling is manifested as a slight reddening of the spectrum of 500-mb geopotential height and a significant enhancement of the lower-tropospheric thermal variance over the oceans at very low frequencies by virtue of the mixed-layer adjustment to surface air temperature variations that occurs on those timescales. This adjustment effectively reduces the thermal damping of the atmosphere associated with surface heat fluxes (or negative oceanic feedback), thus increasing the thermal variance and the persistence of circulation anomalies.

In studying the covariability between ocean and atmosphere it is found that the dominant mode of natural atmospheric variability is coupled to the leading mode of SST in each ocean, with the atmosphere leading the ocean by about one month. The cross-correlation function between oceanic and atmospheric anomalies is strongly asymmetric about zero lag. The SST structures are consistent with direct forcing by the anomalous heat fluxes implied by the concurrent surface air temperature and wind fluctuations. Additionally, composites based on large amplitude SST anomaly events contain no evidence of direct driving of atmospheric perturbations by these SST anomalies. Thus, in terms of the spatial organization of the covariability and the evolution of the coupled system from one regime to another, large-scale air–sea interaction in the model is characterized by one-way atmospheric forcing of the mixed layer.

These results are qualitatively consistent with those from an earlier idealized study. They imply a subtle but fundamental role for the midlatitude oceans as stabilizing rather than directly generating atmospheric anomalies. It is argued that this scenario is relevant to the dynamics of extratropical atmosphere–ocean coupling on intraseasonal timescales at least: the model is able to qualitatively reproduce the temporal and spatial characteristics of the observed dominant patterns of interaction on these timescales, particularly over the Atlantic.

1. Introduction

The question of whether midlatitude sea surface temperature (SST) anomalies can exert an influence on the overlying atmosphere is crucial from the point of view of atmospheric predictability. A related issue is whether the interaction between the extratropical oceans and the atmosphere helps configure the spatial and temporal characteristics of the observed midlatitude low-frequency atmospheric variability. While it has been established that large-scale tropical SST anomalies such as those associated with El Niño–Southern Oscillation (ENSO) can have an impact on the extratropical circulation, there is currently no consensus on whether or not the atmospheric flow is equally sensitive to midlatitude SST anomalies. One view holds that the midlatitude oceans are a slave to the atmosphere and are unable to exert a back-interaction onto the atmosphere. The opposing view contends that coupling in midlatitudes is a cooperative two-way process, and that midlatitude SST anomalies can potentially force anomalous atmospheric circulations and thus be directly responsible for some of the low-frequency variability.

One can find partially supporting evidence for both opinions in observational and modeling studies, as research in both directions has progressed in parallel, yielding a plethora of often contradictory and confusing results, a comprehensive review of which can be found in Frankignoul (1985). From an observational standpoint, it has been known for quite some time that synchronous correlations between midlatitude SST anomalies and atmospheric circulation can be significant in certain regions and during certain seasons (e.g., Namias 1973; Davis 1978). Many of these studies recognized

* Joint Institute for the Study of the Atmosphere and Ocean. Contribution Number 371.

Corresponding author address: Dr. Ileana Bladé, JISAO, Box 354235, University of Washington, Seattle, WA 98195.
E-mail: ileana@atmos.washington.edu

that these correlations are not directly interpretable in terms of cause and effect, nor can the possibility that the correlations have an external origin be excluded (Barnett 1981). Lag-correlations or correlations based on SST tendency generally indicate that the atmosphere is driving the ocean, at least on intraseasonal timescales (e.g., Wallace et al. 1990; Cayan 1992; Deser and Timlin 1997). Yet, one can also find numerous reports in the literature that some midlatitude SST anomalies are linked to atmospheric circulation anomalies at a later time, in so far as they can serve as efficient predictors of short-term climate change in certain regions (Barnett and Somerville 1983)—though, again, the exact cause of this predictability is not well understood.

On the other hand, prognostic-depth mixed-layer models forced with observed surface atmospheric fields have had a surprising success at hindcasting not only the spatial distribution of the variability but even the temporal evolution of intraseasonal to interannual SST anomalies (Haney 1985; Battisti et al. 1995). This would argue in favor of the passive view of the ocean, were it not for the fact that the forcing fields implicitly include the effect of coupling, so that conclusions regarding cause and effect are largely irrelevant.

Conversely, the results from some recent high-resolution GCM experiments with prescribed SST anomalies have reinforced the notion that the atmospheric flow can react to *certain* SST anomalies (Palmer and Sun 1985; Ferranti et al. 1994; Latif and Barnett 1994; Peng et al. 1995). They have also fostered awareness that the mechanisms involved in the atmospheric response to a midlatitude SST anomaly are fundamentally different from the thermally direct circulation with which the atmosphere responds to a tropical SST anomaly. Transient eddy forcing appears to play a pivotal role, which may explain the failure of low-resolution models to exhibit a robust response to extratropical SST anomalies (Kushnir and Held 1996).

Yet, even among those GCMs that predict a robust atmospheric response to a midlatitude SST anomaly there are puzzling inconsistencies in the magnitude and nature of this signal. What to make, for instance, of the nonlinear responses found in Peng et al. (1995)—the model reacts only to a *warm* SST anomaly—or the enormous PNA-like response (i.e., resembling the Pacific–North American pattern) to a modest Pacific SST anomaly in Latif and Barnett (1994)? In addition, the relevance of such prescribed SST experiments to the coupled problem is not clear, because of air–sea feedbacks, which could damp the SST anomaly, and mostly because the atmospheric forcing of the ocean is ignored. It is a fundamental question whether an atmospherically driven SST anomaly can elicit a response that is distinctly different from the perturbation that forced it in the first place. In particular, in view of the similarity between the response to an SST anomaly and the natural variability of the atmosphere (Palmer and Sun 1985), it is reasonable to wonder whether the atmosphere might not so much ''respond'' to the SST but rather adjust or reorganize.

The work of Barsugli (1995) must be credited for first posing the problem in these novel terms. By comparing the variability in a simple zonally symmetric model of the atmosphere coupled to a slab mixed layer with the ''natural'' variability present under fixed SST conditions, he concluded that the main role of this *adjustable* midlatitude mixed layer was to attenuate the damping of low-frequency temperature anomalies. Furthermore, because the enhancement in the thermal variance approximately doubled that in a ''one-way'' driven simulation in which the atmosphere was subject to the time-varying SST forcing from the coupled experiment, he determined that the effect of coupling was ''above and beyond the effect of direct forcing by the SST anomalies.'' This result implies that model experiments that use observed SST as the lower boundary condition cannot give a full representation of the impact of the midlatitude oceans on the atmospheric variability. Barsugli (1995) argued that coupling would qualitatively modify the natural atmospheric variability by ''selectively enhancing'' those components that are more sensitive to thermal damping. This mechanism appears to be generic enough that it should also manifest itself in a more realistic model with a seasonal cycle, land–ocean contrasts, snow–ice distributions, ocean dynamics, etc.

A partial field test for these ideas may be found in a study by Delworth (1996), who performed a series of long, seasonal, coupled GCM integrations with emphasis on Atlantic SST variability. His primary mode of winter-mean atmospheric variability remained essentially unaltered whether the atmosphere was subject to a prescribed annual cycle of SST or was coupled to either a mixed-layer or a full dynamical model of the Atlantic. Feedback from the ocean did not appear to be crucial for the spatial structure of this dominant mode of variability, but no comprehensive assessment of the quantitative and qualitative changes in the atmospheric low-frequency flow was attempted.

The goal of this paper is, on one hand, to establish whether Barsugli's (1995) results can be extended to a more realistic simulation, with land–sea contrasts and time-mean zonal asymmetries. In so doing we will also expand Delworth's (1996) study in order to quantify the changes in the spatial and temporal structure of the low-frequency atmospheric variability as a result of coupling, and assess the extent to which midlatitude SST anomalies help configure the statistical properties of the atmospheric flow. Furthermore, we wish to investigate the characteristic patterns of covariability between the atmosphere and midlatitude oceans and their lead/lag relationships, with emphasis on how they compare to observations. Finally, we want to address the issue of whether large amplitude SST anomalies can induce a direct atmospheric response in a coupled scenario. In Part I, we will consider these questions in the absence of interannual variations in tropical SST. In Part II, we

will introduce tropical Pacific SST forcing with realistic temporal and spatial scales in order to examine, among other issues, the relationship between extratropical SST and hemispheric circulation in the presence of explicit interannual variability.

The model used here is the same low-resolution atmospheric GCM employed in Delworth (1996), coupled to a slab mixed layer and run in perpetual January mode. Though a higher-resolution, fully coupled, atmosphere–ocean GCM would be desirable (especially in light of the above-mentioned findings from fixed SST experiments), emphasis here is placed on obtaining statistically significant results (i.e., long integrations), which currently cannot be afforded except with simplified models. Our intent is to develop a physical intuition for how the midlatitude coupled atmosphere–ocean system operates and to provide a baseline against which future experiments with more detailed, higher-resolution, models can be compared.

This paper is organized as follows. Section 2 presents a brief description of the model and experiments. In section 3 we analyze the changes in the variance of the geopotential height and temperature fields induced by coupling, while section 4 discusses the organization of SST variability. The characteristic patterns of covariability are examined in the next section; this is followed by a comparison with observations and a discussion on the potential role of the ocean in maintaining and generating atmospheric variability. The final section synthesizes the results and attempts to bring them into perspective with respect to observational and other modeling studies.

2. The model and experimental design

The simulations were conducted at the NOAA Geophysical Fluid Dynamics Laboratory (GFDL), using a recent version of their spectral GCM, which includes a cloud prediction scheme by Wetherald and Manabe (1988). There are nine discrete sigma levels in the vertical, while in the horizontal variables are rhomboidally truncated at wavenumber 15 (see Lau 1985; Lau and Nath 1990).

Two very long perpetual January integrations were performed. The first one was 100 200 days long and had fixed climatological mean winter SST boundary conditions; this is our control run (CTRL). Soil moisture, sea ice, and snow depth are also kept fixed at their ''standard'' climatological values (as obtained from a previous seasonal control experiment) so that there are no sources of climatic variability external to the atmosphere itself. In the second experiment (ML) a 50-m-deep motionless slab mixed layer in midlatitudes (from 20° to 56° in both hemispheres) was coupled to the GCM's atmosphere, while elsewhere climatological SST values or sea-ice temperatures were used. The mixed layer interacts with the atmosphere through exchange of surface heat and radiative fluxes. The former are computed using bulk aerodynamic formulas. The simulated time-mean SST is constrained to resemble the observed fields by means of prescribed corrective fluxes that are constant in time and are based on the CTRL climatology[1] (see Lau and Nath 1996 for details on this procedure). From examination of the CTRL simulation it was judged that 40 200 days would be sufficient to attain statistically significant results in the ML experiment.

All analyses described herein are confined to the Northern Hemisphere (NH) extratropics (20°–90°N). Principal component and singular value decomposition analysis is based on latitude-weighted covariance (or cross-covariance) matrices.

3. Atmospheric low-frequency variability

The climatology of the coupled ML experiment exhibits only minor departures relative to that in the control simulation. The time-mean upper-tropospheric fields (not shown) illustrate that while the structure of the simulated planetary wave pattern is close to the observed, its amplitude is too weak, in particular over eastern North America and the Atlantic (30%–40% weaker). This deficiency is common to low-resolution models and is due to the rather flat representation of the orography (in particular the Rockies) at this spectral truncation. Likewise, the climatological east Asian and western Atlantic jets are too weak by about 10 m s^{-1} (not shown).

a. 500-mb height

The spatial distribution of 90-day mean variance of 500-mb geopotential height from the CTRL run is presented in Fig. 1, together with the corresponding difference map between the ML and CTRL experiments. The changes in low-frequency variance brought about by the inclusion of the mixed layer are positive wherever statistically significant. The strong correspondence between the two maps indicates that the variance tends to increase in those regions where it is already large—that is, Alaska, Greenland, and the exit regions of the climatological jets. Note that the R15 GFDL model does a poor job of reproducing the observed variability: in reality the wintertime seasonal variance displays a prominent maximum downstream of the Asian jet core and a weaker secondary maximum southwest of Greenland, with little variance over Alaska. The absolute differences in Fig. 1b translate into small relative increments on the order of 10%–20%, with the most statistically significant (20%–25%) being found over the western Atlantic and east Asia. The increase in hemispherically integrated variance of 90-day

[1] Although this flux correction is designed to minimize its impact on SST variability, this issue has not been investigated in depth.

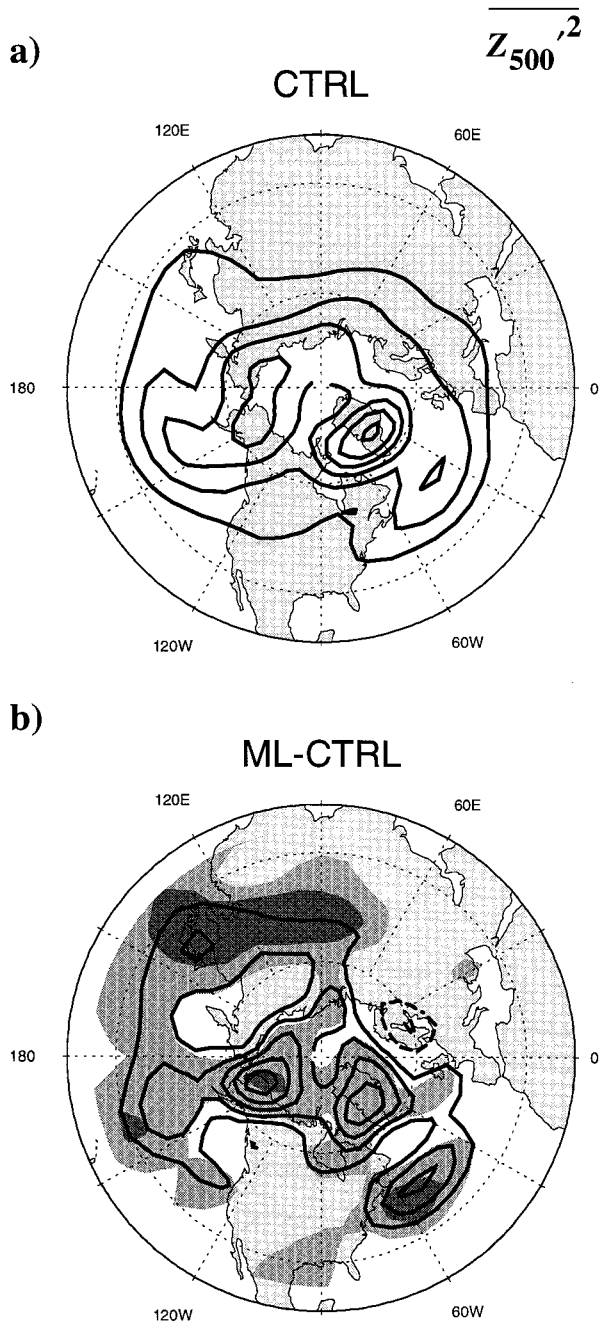

FIG. 1. (a) Variance of 90-day mean geopotential height at 500 mb in the CTRL experiment. Contour interval is 600 m^2. (b) Absolute difference between the 90-day mean variance of 500-mb geopotential height in the ML and CTRL experiments. Contour interval is 100 m^2 with the zero contour omitted; negative contours are dashed. The light and dark shadings indicate regions where the corresponding relative differences exceed 10% and 20%; this corresponds approximately to the 90% and 99% levels of statistical significance for the ratio of variances, based on an F distribution and assuming that all samples are independent.

means is 9.4%, and only slightly larger if the calculation is restricted to grid points over the midlatitude oceans. Corresponding values for longer-term means do not exceed 20% (Fig. 2a).

To examine the impact of the midlatitude SSTs on the spatial organization of the low-frequency variability, we introduce in Fig. 3 the four leading empirical orthogonal functions (EOFs) of the 90-day means of geopotential height at 500 mb for the CTRL experiment. The first EOF, which explains over twice as much variance as the next mode, exhibits a large longitudinally symmetric component, with a node near 50°N. This dominant EOF appears to be the zonally symmetric ''vacillation'' or ''zonal index'' mode (Rossby et al. 1939) that is found in the idealized models of Robinson (1991) and Yu and Hartmann (1993), modulated by the planetary stationary waves.[2] Though such a zonally symmetric mode has an observational counterpart in the sea level pressure (SLP) field (Wallace and Gutzler 1981) and in the upper-tropospheric Southern Hemisphere height field (Karoly 1990), it is not dominant at high levels in the NH. The preponderance of the ''index cycle'' (Namias 1950) in the model can be attributed to the relatively small amplitude of the planetary stationary waves, as well as to insufficient transient eddy activity (again due to the low model resolution), both of which result in insufficient generation of zonally asymmetric low-frequency variability.[3] It is one of the most important weaknesses of these simulations. Nonetheless, this mode bears some resemblance to the observed leading EOF in the sense that they are both associated with a longitudinally symmetric pattern of geostrophic zonal wind anomalies across the central oceans, with fluctuations of opposite sign around 55° and 35°N.

The second EOF is also of planetary scale, with another dipole over the Atlantic. The next two EOFs consist of wave trains over the Pacific–North American region and Eurasia. All of these modes appear to be robust, physically meaningful entities according to the separation criterion proposed by North et al. (1982). They also emerge as the dominant structures of the monthly mean and annual-mean variability. The leading EOF, in particular, remains virtually identical for any averaging interval ranging from 10 to 1000 days (Nitsche 1996).

The corresponding patterns for the ML experiment are so similar to the ones shown in Fig. 3 that we will not present them. Minor differences can be seen in the location of the centers of action of the higher-order EOFs

[2] This mode depends strongly on eddy-mean flow interactions for its existence. The modulation by the stationary waves occurs through the action of the high-frequency transient eddies in the jet exit regions, resulting in maximum amplitudes over the mid-Atlantic and Pacific Oceans. In Yu and Hartmann (1993) this mode had an equivalent barotropic structure. Analysis of the 200-mb streamfunction and sea level pressure fields suggests that this mode is also largely equivalent barotropic in the current model (see Nitsche 1996 for more details).

[3] This mode may also be weakly resonant.

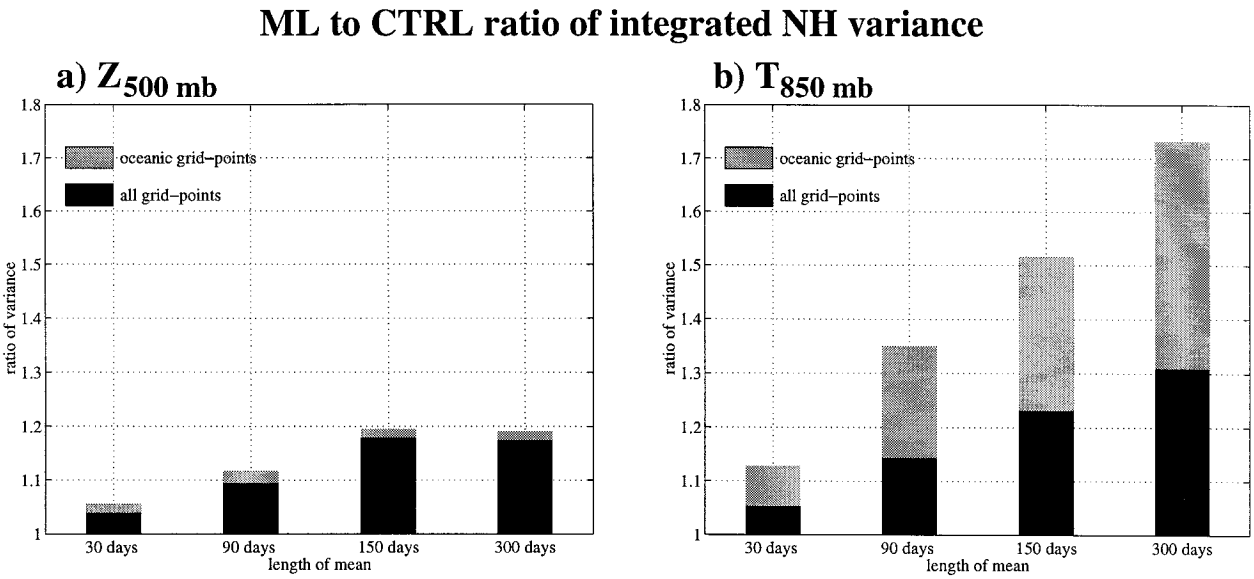

FIG. 2. (a) Ratio of total variance of 500-mb geopotential height in the mixed-layer experiment to that in the control experiment as a function of averaging length. The black columns refer to the total (area weighted) NH variance poleward of 20°N; the gray columns refer to the total (area weighted) variance over the NH extratropical (20°–56°N) mixed-layer ocean. (b) Same but for temperature at 850 mb.

(pattern correlations $r \geq 0.92$), but the leading EOF is indistinguishable in the two simulations ($r = 0.99$). No new reproducible structures (according to the aforementioned criterion), intrinsic to the ML run, emerge in this or any other frequency range, nor is the ordering of the EOFs affected by the presence of a mixed layer. The only noticeable change is that the leading EOF explains a slightly larger fraction of the total variance in the ML run (see Fig. 3). Not only is the variance enhancement in the coupled experiment unequally distributed among the EOFs, but it is mostly concentrated in the first two modes: the amount of total 90-day mean variance accounted for by individual modes increases by 20% for the leading EOF, 10% for the second EOF, and remains similar for the other modes. The tendency for the leading EOF to be preferentially amplified by the coupling is even more evident for longer-term means (not shown).

Shown in Fig. 4a is the power spectrum of the principal component of EOF-1 calculated from monthly mean data for both experiments. These spectra were obtained by averaging over individual realizations of 134-month length (hence 24 realizations in the CTRL run and 10 in ML). It is evident that only in the 14–134-month band is the variance in ML significantly larger than in CTRL. Related to this accentuated redness in the spectrum of the leading EOF is an incremental increase in the autocorrelation at all lags (Fig. 4b). There may also be a slight tendency for a higher frequency of persistent extreme EOF-1 events: for instance one finds 13 episodes in the ML experiment in which the amplitude of EOF-1 exceeds two standard deviations during two or more consecutive months, versus 10 (on average) in the CTRL run during an equivalent time period.

Clearly, the impact of midlatitude air–sea coupling on the variability of the midtropospheric geopotential height field is weak. It appears that the spatial structure of the variability is not noticeably altered when the atmosphere is allowed to interact with midlatitude SSTs. The main influence of the mixed layer is to redden the spectrum of the variability, but this effect is modest and largely confined to the leading EOF. We now examine the effects on the thermal variance.

b. 850-mb temperature

In contrast with the small changes in the geopotential field, the inclusion of a mixed layer results in a substantial enhancement of the thermal variance at low levels. This increase is again felt only at the lowest frequencies and is much more pronounced over the oceans (Fig. 2b). Figure 5 shows the spatial distribution of the ratio between the variance of 300-day mean temperature at 850 mb in ML and that in CTRL. Over a small area in the central Pacific the ratio exceeds 2.5 but is generally indicative of a (statistically significant) 50% to 100% increase over the midlatitude oceans, while over the continents the increase is smaller than 25% in most places and locally not significant. Ratios of spatially integrated variance for various averaging lengths are displayed in Fig. 2b.

Figure 6a shows the frequency spectra of 850-mb temperature averaged over all oceanic grid points at 38°N (the latitude of maximum change in 300-day mean variance in the central Pacific). These spectra were obtained by constructing pentad time series from the daily output file, then applying the spectral analysis to nonoverlapping 800-pentad-long segments, and averaging the resulting spectra over all realizations and longitudes.

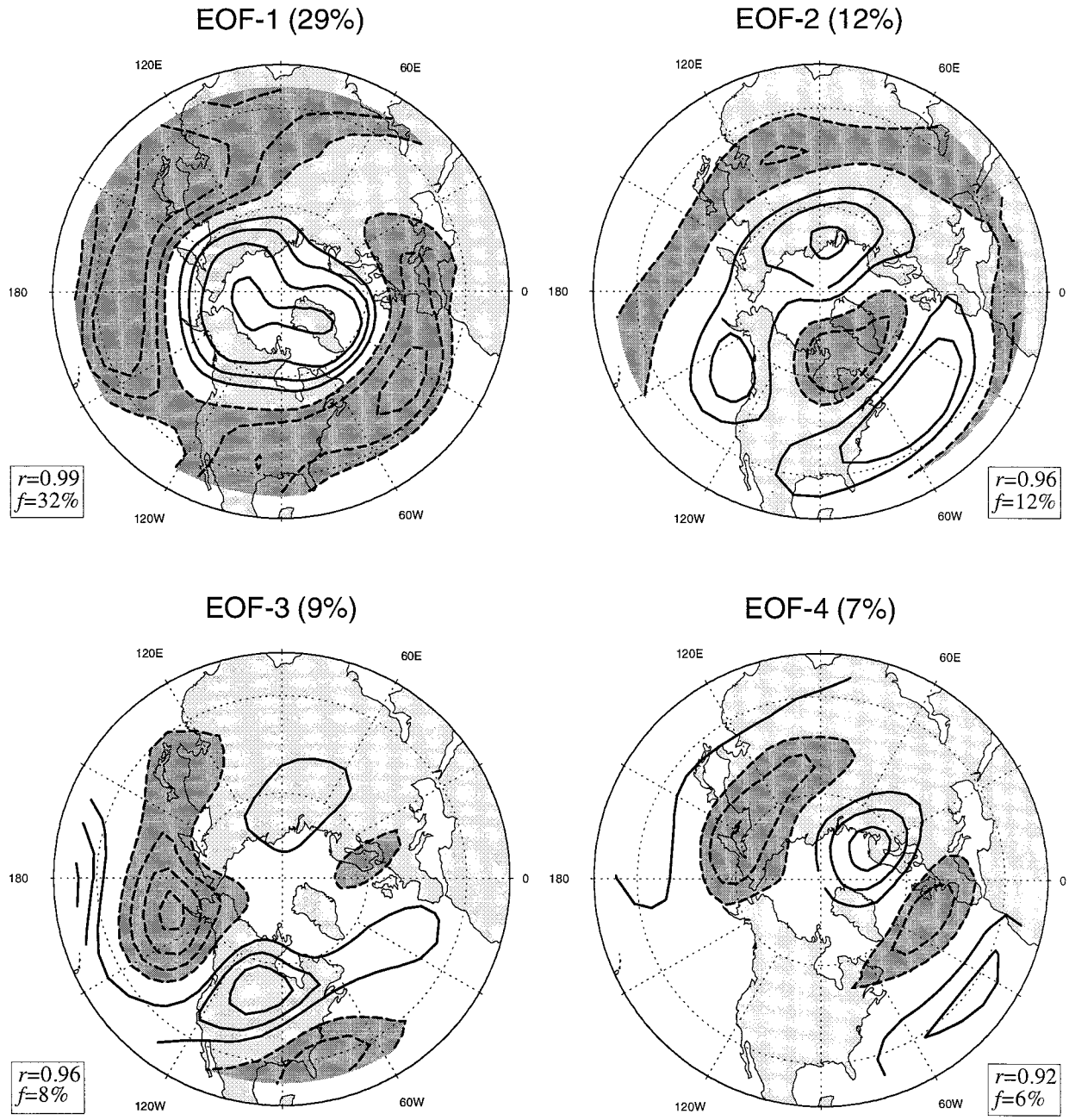

FIG. 3. The four leading EOFs of 90-day mean geopotential height at 500 mb in the CTRL experiment, presented as the correlation coefficient between the principal component time series and the time series of 500-mb height at individual grid points. Contour interval is 0.2, with the zero contour suppressed. The dark shading indicates correlations less than −0.2. The numbers in parenthesis denote the percentage of hemispherically integrated variance explained by that mode. The corresponding EOFs for the ML experiment are very similar, as indicated by the spatial correlation between the patterns *r*, which is shown at the bottom of each panel; also shown is the percentage of total variance *f* explained by that EOF in the ML experiment.

It is clear that even for oceanic grid points, the increase in variance in the coupled run is manifested only at very long periods (400 days or longer). This enhancement in the ultra-low-frequency thermal variability appears to be associated with the eastward propagating long wavenumber components ($k = 1 - 2$), as can be inferred from Fig. 7, which presents the difference between the wavenumber-frequency spectra at 38°N in ML and CTRL. Consistent with these changes, we also observe a distinct tendency for enhanced persistence of temperature fluctuations over the oceans: the one-lag autocorrelation of monthly means (Fig. 8) increases from values around 0.05 to near 0.2 over most of the central oceans. On the other hand, the spatial structure of the

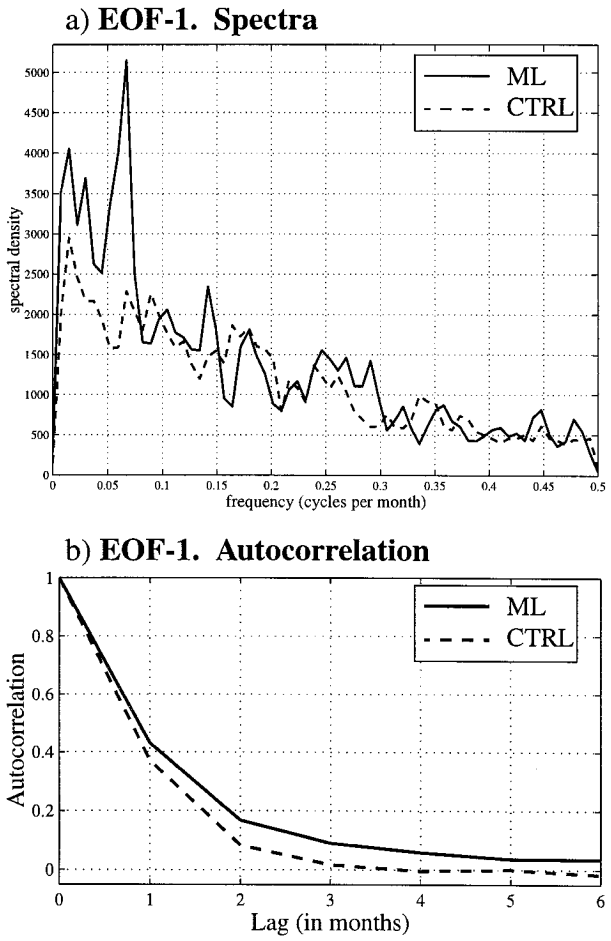

FIG. 4. (a) Power spectra of the principal component of the leading EOF of monthly mean 500-mb geopotential height for the ML and CTRL experiments (note that its structure is identical to that of the leading EOF of 90-day means, shown in Fig. 3). The spectra were computed using a Hanning window and averaging over 10 and 24 realizations, respectively, with the lowest-frequency 1/134 months. (b) The corresponding lag-autocorrelation function in the two experiments.

thermal variability (as represented by the leading EOFs) is again not noticeably modified by coupling.

These results, which indicate that the effect of coupling is felt only locally and at very low frequencies, are in agreement with those obtained by Barsugli (1995) in an idealized study and by Manabe and Stouffer (1996) using this same model. Barsugli's two-level model, which has an all-ocean geometry, undergoes a 54% enhancement in the low-frequency (200–2000 days) variance of vertically averaged temperature in midlatitudes when coupled to a slab mixed layer but only a 12% rise in overall variance. Manabe and Stouffer (1996) performed multiyear seasonal integrations of the GFDL GCM combining it with either a mixed layer or a full dynamical ocean; they observed an amplification of about 50% (60%) in the standard deviation of annual (5-yr mean) surface air temperature over the midlatitude oceans in both coupled experiments (compared to their fixed SST experiment) and little change over the continents. Gallimore (1995) reported a similar effect of including an interactive mixed layer in his low-resolution model; since he considered only monthly mean anomalies, however, the impact on the thermal variability was very small.

It is helpful to examine the spectral distribution of surface heat fluxes in order to understand the increase in low-frequency thermal variance in the coupled experiment. Spectra for the total heat flux at the ocean surface were computed from monthly mean data, using a similar window to that in the temperature spectra, and are presented in Fig. 6b. For relatively short periods between 100 and 450 days the power density of surface fluxes is somewhat lower in the ML run than in the CTRL run but exhibits the same weak frequency dependence. For periods longer than 450 days, however, the ML spectrum decreases as the frequency goes to zero, in sharp contrast with the CTRL spectrum for which the power is maximum (or remains high) at the lowest frequencies. Note that because the effect of wind speed variations on the surface fluxes is small, in the control simulation these act essentially as a damping on the lower temperature field (the correlation between downward fluxes and $T_{850\ mb}$ is large and positive everywhere).

As discussed by Barsugli (1995), this attenuation of the surface heat fluxes at low frequencies in the coupled experiment simply reflects the *adjustment* of the ocean to surface air temperature fluctuations that occurs on timescales longer than the decorrelation time of the mixed layer (about 4 months). Because of this adjustment, the thermal damping of the atmosphere by the ocean, or negative oceanic feedback, which is strong when the SST is kept fixed, is considerably reduced, especially at the very low frequencies for which the adjustment is nearly complete. It follows that the atmospheric thermal variance at these frequencies will increase. In space, it is in the central areas of the midlatitude oceans, near the regions of greatest atmospheric wave activity, where the cumulative effect of this decreased damping is felt the most, hence, the localized maxima in Fig. 5.

The preferential enhancement of the leading mode of 500-mb height may also be partially understood as a result of its having maximum amplitude and maximum area coverage over the oceans. Furthermore, Fig. 7 suggests that the reduction in thermal damping is most effective for the longest waves. This is consistent with the fact that the first and second EOFs are selectively amplified by the coupling, since these patterns are of predominantly large scale (strong $k = 2$ and $k = 1$ components, respectively) compared to the also partially maritime but shorter wavelength EOF-3 (Fig. 3).

4. Sea surface temperature variability

Figure 9 shows the standard deviation of monthly mean SST in ML. In qualitative agreement with obser-

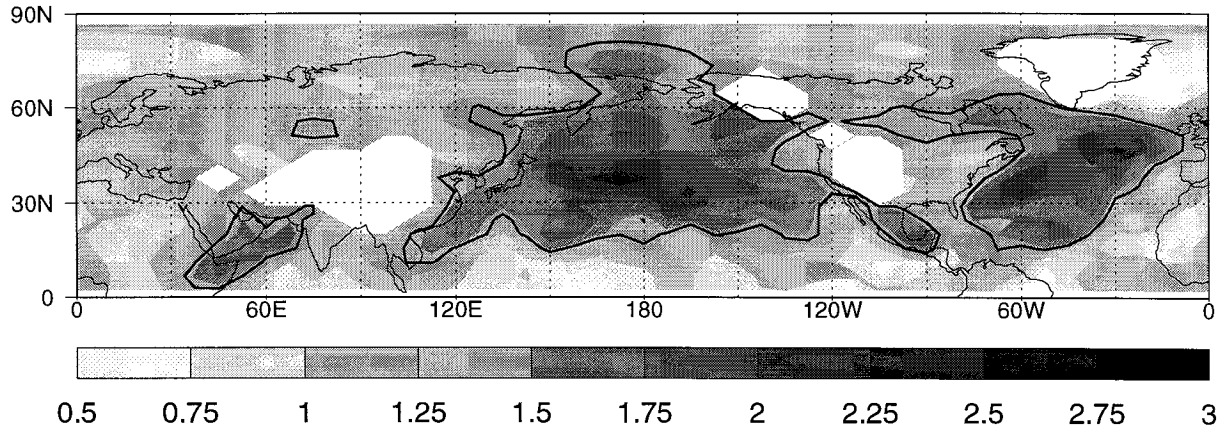

FIG. 5. Ratio of variance of 300-day mean temperature at 850 mb in the ML experiment to that in the CTRL experiment. Shading contour is 0.25, with the darker shadings indicating ratios larger than 2. The white areas indicate mountainous regions where the 850-mb surface is not always defined. The black line is the 1.4 contour, which represents the 99% significance level, based on an F distribution and assuming all samples are independent, or alternatively, the 95% level assuming one in every two samples is independent.

vations, the standard deviation is largest along the northeastern coast of the continents, that is, the regions subject to frequent incursions of anomalously cold continental air and more susceptible to warming due to anomalous easterly or southerly flow. The simulated anomalies, however, are generally too weak in midlatitudes (by as much as 50% in the coastal regions and central North Pacific), and the large anomalies along the sea–ice interface appear to be an artifact of the model resulting from the fixed sea-ice temperatures. Only in the central and eastern North Atlantic do the SST departures exhibit realistic magnitudes. At least part of this missing variability is related to the absence of oceanic processes in our simple mixed-layer ocean, while the lack of remote tropical SST forcing in the Pacific also contributes to the underestimation of the SST variability. This latter effect will be investigated in part II. For now, though, we are concerned with examining how an *atmospherically driven* oceanic mixed layer modifies the *intrinsic* midlatitude atmospheric variability, irrespective of any tropical SST effect.

The two leading EOFs of monthly mean SST in the Atlantic and Pacific regions, which explain approximately half of the total variance in each ocean, are presented in Fig. 10. These dominant patterns are of basin-wide scale while the higher modes (not shown) display progressively smaller spatial scales, in agreement with observations. In both oceans the first EOF is characterized by a zonally elongated band extending along the ~25°–45°N latitude belt, flanked by a narrower anomaly of opposite polarity to the north, with maximum amplitudes in the western part of the basin. In the Atlantic, this structure (which alone accounts for 42% of the variance) bears a distinct similarity to the observed leading pattern (Wallace et al. 1990), with even a hint of a third southwest–northeast-oriented strip in the subtropics (recall that the model's mixed layer does not extend south of 20°N). The greater prominence of the northern center of action in the model is probably due, in part, to too shallow a mixed layer at that latitude, as argued by Delworth (1996). Furthermore, this mode is not as overwhelmingly dominant in the real atmosphere as in the model. Delworth's (1996) seasonal integration with the same atmospheric GCM coupled to a global mixed layer yields a pattern similar to that in Fig. 10 (between 20° and 56°N) but less dominant as well—a reminder that the leading mode of atmospheric variability (which, we will show, is responsible for this SST pattern) is unrealistically important in our perpetual winter integrations.

In the Pacific sector, the zonally symmetric, dipolar, leading SST pattern is less prominent and does not resemble its observational counterpart; its general structure, however, is broadly similar to that of the second EOF of observed Pacific SST, believed to be associated with internal midlatitude variability (Deser and Blackmon 1995). The fact that the observed leading mode is not reproduced in this simulation is consistent with the fact that the midlatitude SST in this ocean is strongly influenced by ENSO, through its extratropical atmospheric manifestation—an effect not included in this study. Both the second Atlantic and Pacific model EOFs are characterized by a large-scale monopolar anomaly that is reminiscent of patterns found in nature [e.g., Peng and Fyfe's (1996) Atlantic S2 mode].

Linear lagged regression maps of SST using the principal component of the leading EOFs as the reference time series reveal a tendency for very slow eastward propagation in the center and eastern part of the basins (Fig. 11). This finding is consistent with Frankignoul's (1985) argument, based on results from a linear quasi-geostrophic β-plane model, that coupling will induce an eastward drift of ''ultralong'' SST anomalies. The phase speeds, however, are on the order of 5 cm s^{-1}, which is lower than predicted by Frankignoul and than what Barsugli (1995) found in his two-level coupled model.

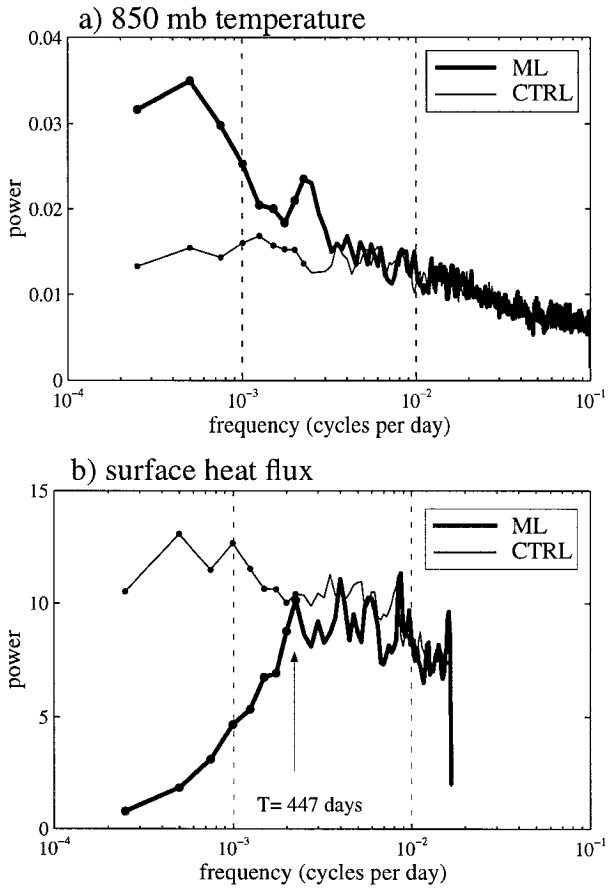

FIG. 6. (a) Frequency spectra of 850-mb temperature at latitude 38°N, averaged over all oceanic grid points. The thick line denotes the spectrum for the ML run, computed using an 800-pentad (or 4000-day) Hanning window (hence 10 individual realizations), while the thin line denotes the corresponding spectrum for the CTRL run (25 realizations). Units are K^2. The dots indicate the individual spectral estimates for the lowest frequencies. (b) Same as (a) but for the total heat flux at the ocean surface. The spectra are computed using a 134-month (or 4020-day) Hanning window (hence 10 realizations for the ML run and 24 for CTRL). Units are $(W\ m^{-2})^2$.

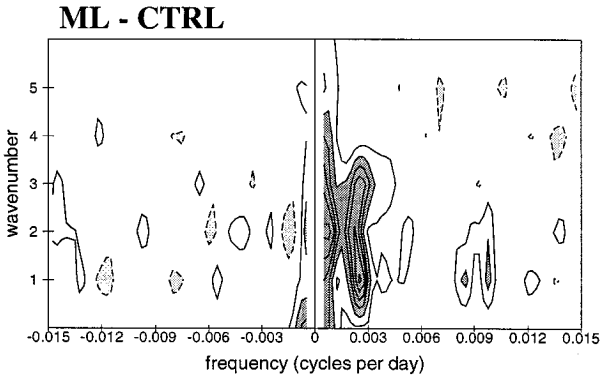

FIG. 7. Difference between the wavenumber-frequency spectra of 850-mb temperature at 38°N in the ML and CTRL experiments, where the spectra have been computed using the same window as in Fig. 6a and including all grid points. The spectra have been smoothed twice with a 1–2–1 filter. Contour interval is 3×10^{-4} K^2. The dark shading denotes differences greater than 6×10^{-4} K^2 and the light shading negative differences greater than -3×10^{-4} K^2.

5. Covariability of the ocean and atmosphere

a. The leading mode

We will investigate the principal (linearly) coupled modes of variability of the atmosphere and the mixed-layer ocean by means of a direct singular value decomposition (SVD).[4] The analysis is first applied to ''seasonally'' (90-day) averaged hemispheric atmospheric fields and Atlantic SST. Figure 12a displays the heterogeneous correlation maps of 500-mb geopotential height and Atlantic SST for the first SVD mode. This mode explains 86% of the total squared covariance and therefore constitutes the prevailing form of coupling between these two fields. The geopotential height pattern projects strongly onto the leading EOF of this field (see Fig. 3; recall that this mode is the same as in the CTRL run), while the SST pattern is identical to the corresponding leading EOF (and to that shown in Fig. 10a). Table 1 illustrates how well the EOFs and SVD patterns for each field are correlated in space and time. Thus, the dominant modes of hemispheric geopotential height and Atlantic SST tend to occur in conjunction. The heterogeneous correlations, though, are rather weak and so is the correlation between the expansion coefficient time series of the two SVD patterns (0.53). This correlation increases to 0.7 (Fig. 13a) and the pattern of heterogeneous correlations strengthens (Fig. 12b) when the atmosphere leads the ocean by one ''season,'' suggesting that the atmosphere is driving the ocean.

The leading SST structure that emerges from corresponding SVD expansions using SLP or temperature at 850 mb as the atmospheric variable is indistinguishable from that in Fig. 12. Again, the relationship is strongest when the SST lags the atmosphere. We thus obtain a thermal and dynamical picture of the surface circulation anomaly pattern that occurs prior to the leading mode of Atlantic SST (Fig. 14). This pattern supports an interpretation in terms of a direct response of the mixed layer to forcing by the atmosphere, in keeping with the lag-autocorrelation results. In the polarities shown, enhanced climatological surface westerlies (tradewinds) near 55°N (25°N) are seen to precede the cold SST anomalies in high (low) latitudes, as one would expect from enhanced evaporation and sensible heat transfer—that is, increased heat flux out of the ocean. Additionally, negative (positive) 850-mb temperature

[4] Note that, as discussed by Newman and Sardeshmukh (1995), in those cases where SVD analysis can successfully retrieve the correct linear relationships between two fields, analogous results can be obtained by correlating the principal components of one variable with the time series of the other. This is indeed the case for the pairs of fields discussed below. The SVD technique, however, provides a more compact and straightforward way of assessing the degree of coupling.

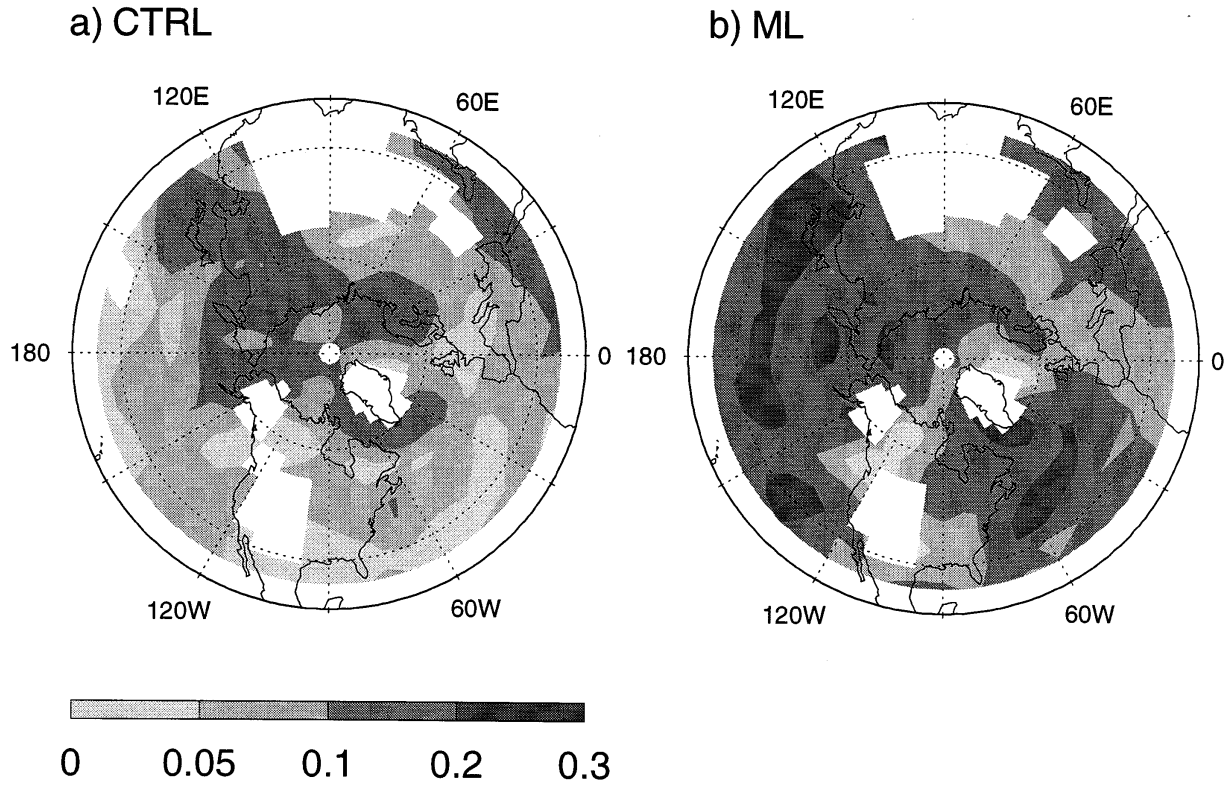

FIG. 8. Autocorrelation of monthly mean temperature at 850 mb in the CTRL (left) and ML (right) experiments. The white areas indicate mountainous regions where the 850-mb surface is not always defined.

anomalies overlay the cold (warm) SSTs. These thermal and accompanying moisture anomalies create anomalous air–sea gradients that again reinforce (lessen) the upward heat fluxes at the ocean surface, leading to the observed SST anomalies.

Delworth (1996) obtained similar patterns of covariability by regressing the time series of the leading EOF of Atlantic SST on the 500-mb height and SLP fields. Moreover, his results essentially duplicated those from another experiment that included a full ocean GCM, indicating that ocean dynamics were not involved in any major way in this dominant form of atmosphere–ocean interaction. We do not wish to repeat Delworth's (1996) diagnosis of the relative contributions from the wind and gradient anomaly terms to the latent and sensible heat fluxes that drive the SST anomalies in Fig. 12. From the configurations of the $T_{850\ mb}$ and SLP patterns relative to that of SST, we anticipate that, as was found in that study, surface air temperature and moisture anomalies play the most important role in generating heat flux variations, with the exception of the subtropics where trade wind variability appears to be solely responsible for the SST anomaly center in the eastern Atlantic. This is consistent with Battisti et al.'s (1995) analysis of observed Atlantic surface heat fluxes and SST.

Over the Pacific Ocean the situation is similar (Fig.

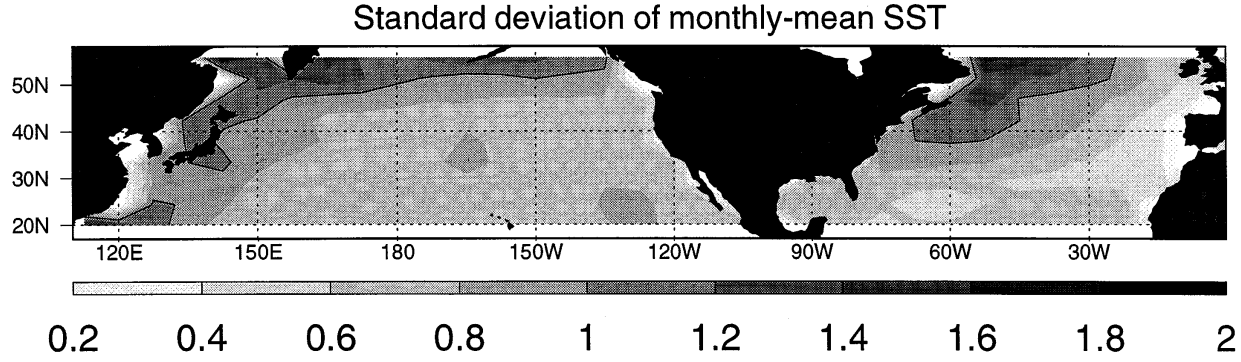

FIG. 9. Standard deviation of 30-day mean SST. Shading contour is 0.2 K. The thin line is the 1 K contour.

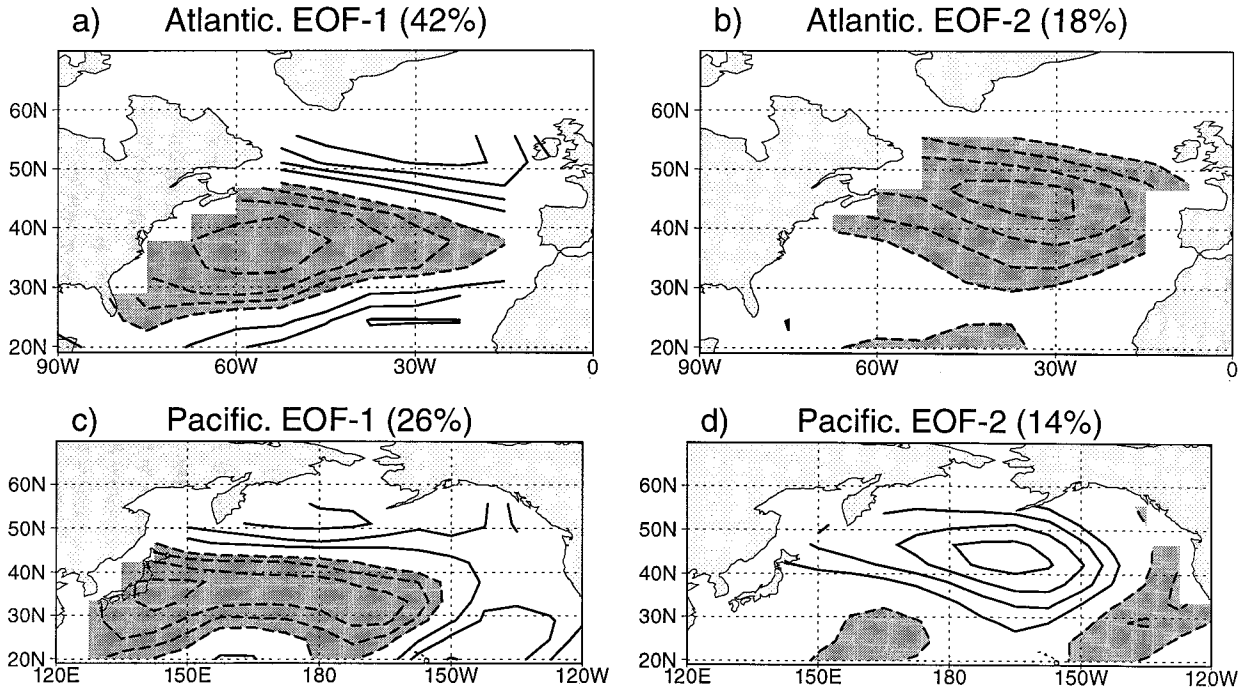

FIG. 10. The two leading EOFs of monthly mean Atlantic (upper panels) and Pacific (lower panels) SST in the ML experiment, presented as the correlation coefficient between the principal component time series and the time series of SST at each grid point. Contour interval is 0.2, with the zero contour suppressed. The dark shading indicates correlations less than −0.2. The numbers in parenthesis denote the percentage of total variance in each ocean explained by that mode. The corresponding patterns for ''seasonal'' (90 day) mean SST are identical. Note that the mixed layer extends only to 56° N.

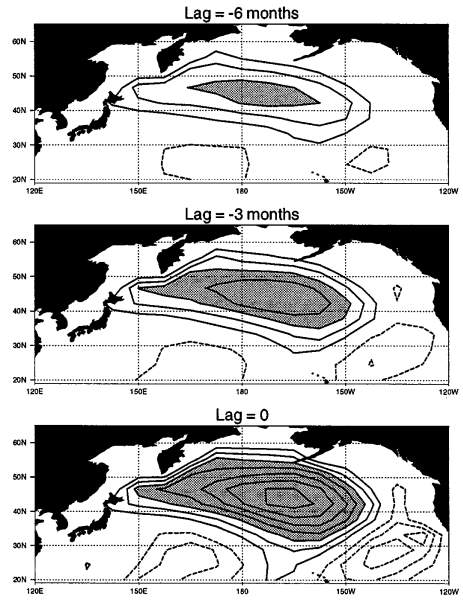

FIG. 11. Linear lagged-regressions of monthly mean Pacific SST onto the principal component time series of the second EOF of Pacific SST, for several lags. Values represent the SST anomalies associated with one (positive) standard deviation in the principal component. Contour interval is 0.12 K; the shading indicates values greater than 0.36 K. The phase speed implied by the eastward expansion of the SST anomalies is approximately 5° long (100 day)$^{-1}$.

13a and Table 1) except that the fraction of total squared covariance (SCF) explained by the first pair of coupled patterns is somewhat lower (75%) and so are the spatial correlations (not shown). The dominant mode of Pacific SST (Fig. 10c) is also diagnosed to be the result of direct forcing by the principal structure of atmospheric variability. Since the dominant SST patterns in each ocean are linked to the same hemispheric mode of geopotential height, one expects these oceanic patterns to be temporally correlated: the correlation is 0.41.

It is worth stressing that this leading mode of atmospheric variability that controls much of the SST activity in both oceans is in fact the principal mode of *uncoupled* low-frequency variability. That is, although the atmosphere interacts strongly with the mixed layer, the ocean is not implicated in the establishment of this prominent form of atmospheric circulation. In the next section we discuss more extensively the role of the ocean in the coupling.

b. Oceanic contribution

As discussed by Frankignoul (1985), the large *simultaneous* correlation between the atmospheric and oceanic anomalies associated with the leading SVD mode in each ocean (Fig. 13a) is to be expected as a result of the inherent persistence of the atmospheric pat-

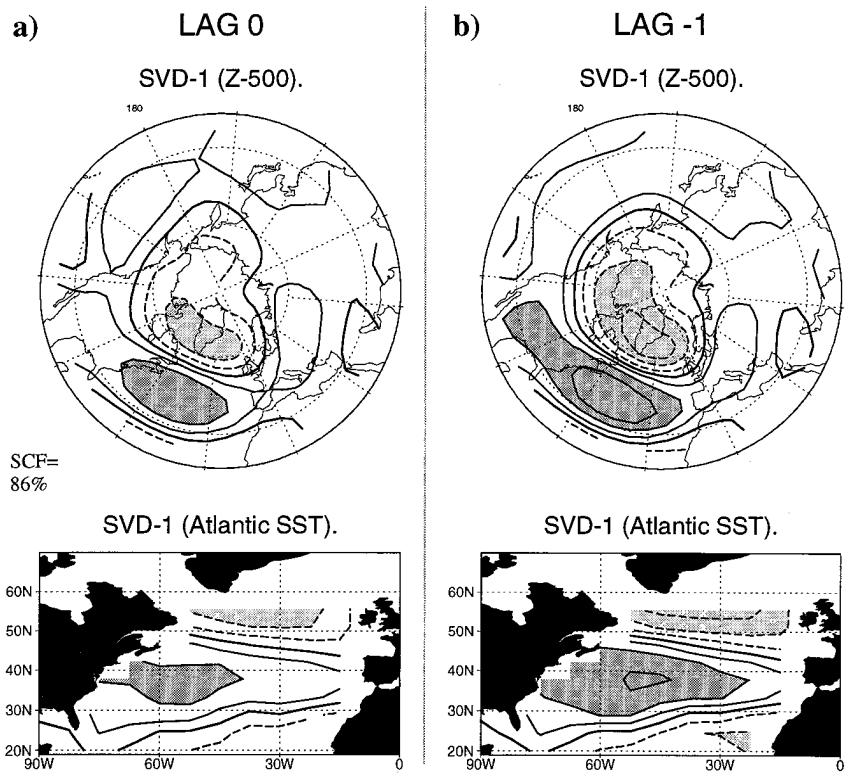

FIG. 12. (a) Simultaneous heterogeneous correlation patterns of 500-mb geopotential height and Atlantic SST for the leading SVD mode, based on 90-day mean data. The contour interval is 0.2; the thick line is the zero contour. Dark (light) shading indicates correlations larger (smaller) than 0.4 (−0.4). SCF refers to the squared covariance fraction explained by this mode. (b) Same as (a) but the correlations are computed for the atmosphere leading the ocean by 1 lag (i.e., 90 days). The maximum values of the corresponding heterogeneous regressions are 42 m and 1 K.

terns as well as the temporal smoothing. It is not indicative per se of a back interaction from the ocean onto the atmosphere. Such information may be contained instead in the correlation for positive lags, that is, for the ocean leading the atmosphere.

According to Frankignoul and Reynolds's (1983) theoretical model of the mixed layer, SST variations in regions of weak mean current can be expressed as a response to a stochastic process F with a short decorrelation timescale, representing the white-noise-like atmospheric perturbations: $dT_s/dt = F - \lambda_o T_s$; λ_o denotes an internal oceanic feedback parameter related to dissipation, radiative damping, etc. The atmospheric forcing F may include an additional ''atmospheric'' feedback component $-\lambda_a T_s$ that describes the linear damping effect associated with surface heat fluxes ($\lambda_a > 0$) and/or parameterizes the potential influence of an SST anomaly on the atmospheric circulation and, indirectly, on the SST anomaly itself ($\lambda_a > 0$ or < 0, depending on the character of the atmospheric response). In the context of this theoretical model, weakly negative cross correlations between atmospheric forcing and SST at positive lags, such as those in Fig. 13a, are indicative of a back-interaction of the SST anomalies on the atmospheric circulation that almost compensates for the negative surface flux feedback; otherwise, the cross-correlation function would be strongly antisymmetric. Increased symmetry and positive correlations at all lags would reflect a net positive ''atmospheric'' feedback ($\lambda_a < 0$).

Strictly speaking, the Frankignoul and Reynolds's stochastic mixed-layer model is not directly applicable to the coupled atmosphere–ocean scenario. As pointed out by Barsugli (1995), a more appropriate model would be a stochastically forced *coupled* model, in which the internal variability of the atmosphere is the stochastic variable and the feedback due to surface fluxes is deterministically incorporated into the model, so that the feedback due to the response of the atmosphere to SST anomalies can be considered separately. Still, if the mixed layer is merely responding to atmospheric perturbations with-

TABLE 1. Spatial (left of slash) and temporal (right) correlation between the patterns associated with the leading SVD mode of 90-day mean hemispheric 500-mb geopotential height and regional SST and those associated with the leading EOF of the respective fields.

	Z-500	SST
Atlantic	0.90/0.96	0.99/0.99
Pacific	0.96/0.99	0.97/0.99

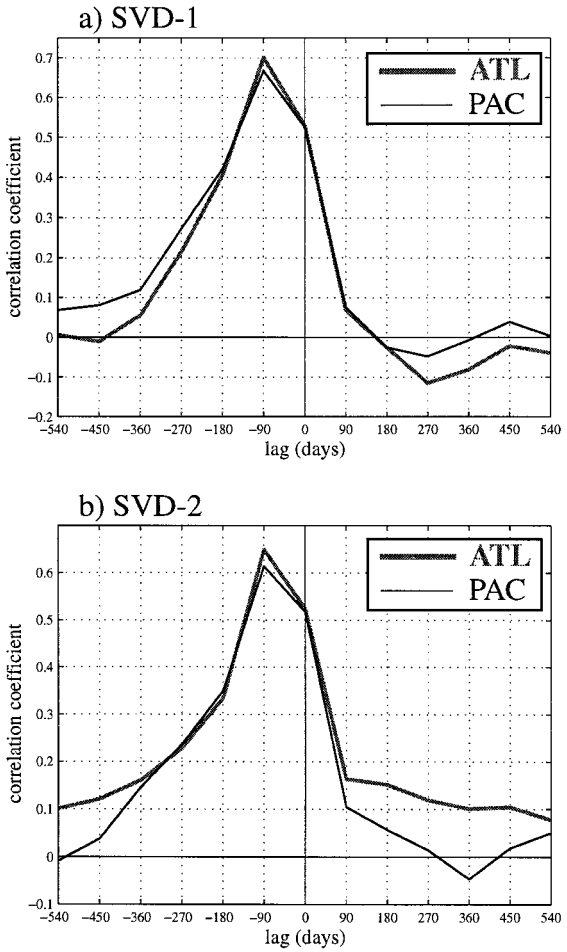

FIG. 13. Lag correlations between the expansion coefficient time series of the patterns of hemispheric 500-mb geopotential height and regional SST associated with the first two SVD modes, computed from 90-day mean data. A negative lag indicates that the atmosphere is leading the ocean. Thick line: Atlantic SST; thin line: Pacific SST. Upper panel: first SVD mode; lower panel: second SVD mode.

out exerting any kind of maintaining influence on them, one can safely say that the correlation will become zero or weakly negative when SST leads, as the heat flux absorbed by the ocean is lost to an essentially ''white'' atmosphere. If instead the two media act to *mutually* reinforce each other, one would expect a more symmetric cross-correlation function that remains finite and positive when SST leads. Such a positive (i.e., unstable) feedback is usually envisioned to involve a *dynamical* response of the atmosphere to the SST anomaly that it has forced; this response then acts to strengthen the initial atmospheric perturbation and hence the SST anomaly. This possibility is suggested by the results of some prescribed SST GCM experiments in which, for instance, a warm SST anomaly induces an anticyclonic response aloft with downward heat fluxes at the ocean surface (Latif and Barnett 1994; Peng et al. 1995).

The results from section 3 indicate that in this model coupling has the effect of prolonging the lifetime of atmospheric anomalies not through dynamical feedback but simply by attenuating the thermal damping due to surface heat fluxes. This should result in somewhat stronger correlations at positive lags than if the coupling between the atmosphere and ocean was purely one way, that is if the mixed layer was passively responding to atmospheric perturbations. This can be easily verified by running the mixed-layer model in diagnostic mode as in Lau and Nath (1996) and Delworth (1996)—that is, by forcing it with the monthly mean fluxes from the CTRL simulation and including a linear damping. The leading atmospheric and oceanic SVD structures that emerge in this one-way forced simulation are very similar to those in the fully coupled simulation ($r > 0.97$); the cross-correlation functions, however, drop sharply to zero at lag 90 days for any reasonable value of the damping timescale (i.e., faster than in ML; not shown).

The differences between these one-way cross-correlation functions and those in Fig. 13a are small, but this is consistent with the fact that the effect of coupling at these relatively short periods (90 days) is weak (recall section 3). If, in addition to this thermal effect, SST anomalies induced a *dynamical* atmospheric response that helped sustain the circulation that forced them, we would have obtained a more symmetric cross-correlation function. Note that this distinction between thermal and dynamic feedback is somewhat artificial since the thermal adjustment of the surface air to the ocean temperature undoubtedly entails some kind of dynamical adjustment in the free atmosphere. If a ''direct'' dynamical two-way interaction was taking place, however, the ocean would play a more active role in selecting the dominant coupled patterns, instead of these being exclusively determined by the dominant form of atmospheric variability.

That the patterns identified in the previous section largely represent the signature of one-way forcing of the ocean by the atmosphere can also be verified by repeating the SVD analysis using SST tendency rather than SST. By construction, this analysis will reflect primarily the atmospheric driving of the ocean. The resulting patterns are virtually identical to those from the earlier calculation ($r > 0.97$, not shown). It is also of interest to perform SVD expansions based on pentad data, which enables us to examine the nature and magnitude of the ''true'' unsmoothed temporal relationship between oceanic and atmospheric anomalies. As expected, this calculation retrieves exactly the same patterns ($r > 0.99$), while the fine-resolution cross-correlation functions display no novel features relative to those based on seasonal data, only weaker magnitudes (not shown). The correlation is maximum (0.5) when the atmosphere leads by 30 days and drops rapidly at shorter lags. The 1-month delay is roughly consistent with the 2–3 week prediction from the simple stochastic forcing model of Frankignoul and Hasselmann (1977), which assumes no atmospheric feedback.

These series of analyses identify, therefore, the same

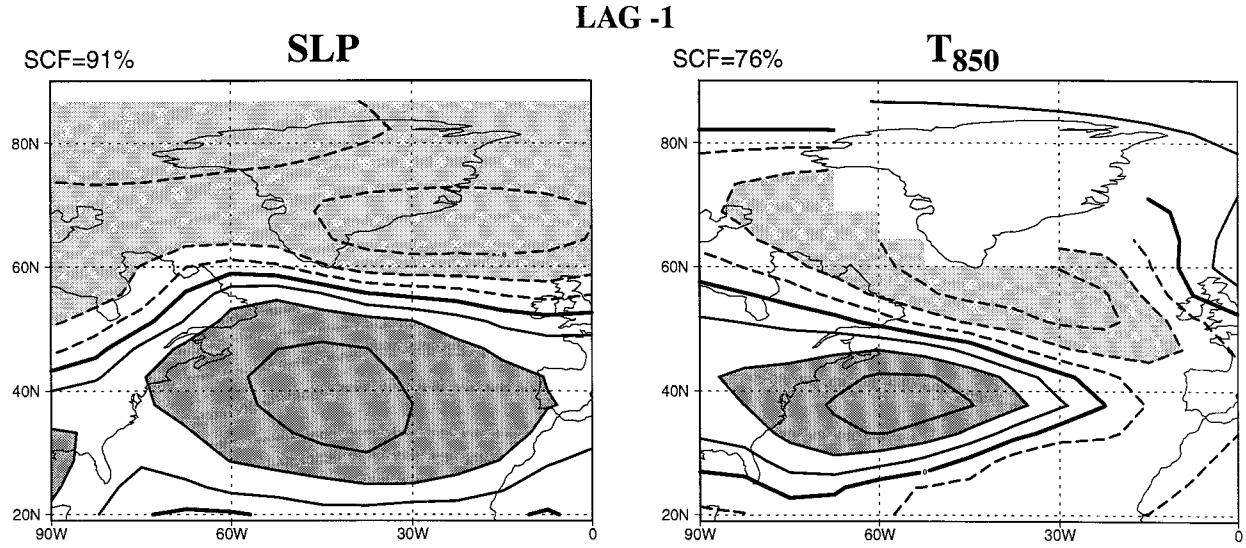

FIG. 14. (Left): Heterogeneous correlation pattern of sea level pressure for the leading SVD mode of 90-day mean sea level pressure and Atlantic SST with the atmosphere leading the ocean by 1 lag. (Right): Same but for temperature at 850 mb. The corresponding patterns of Atlantic SST are identical to that in Fig. 12b (spatial and temporal correlations > 0.99) in the polarity shown. The contour interval is 0.2; the thick line is the zero contour. Dark (light) shading indicates correlations larger (smaller) than 0.4 (-0.4).

kind of essentially one-way large-scale air–sea interaction. The ocean is not an idle participant, since it allows atmospheric perturbations to persist for somewhat longer than they would in the absence of oceanic adjustment. There is, however, no indication of an unstable *dynamical* feedback between the SST anomalies and the atmospheric circulation that generates them.

c. Comparison with observations

Several studies have explored the observed dominant large-scale patterns of extratropical atmosphere–ocean interaction using statistical techniques analogous to those employed here. Wallace et al. (1990, 1992) applied principal component and SVD analysis to winter-mean hemispheric 500-mb height and regional SST data. Because the coupling patterns based on SST were noticeably different from those based on SST tendency, they conjectured that the simultaneous correlations between SST and 500-mb height were a reflection of a two-way interaction between the atmosphere and ocean, thereby defying a simple explanation regarding cause and effect. On the other hand, the patterns of association between SST tendency and $Z_{500\ mb}$—zonally oriented band like structures reminiscent of those in our simulation—lent themselves to a direct interpretation in terms of atmospheric forcing of the ocean, accomplished through the modulation of surface heat fluxes, entrainment, and vertical mixing by the atmospheric circulation. Thus, on interannual and longer timescales, it would appear that the situation is more complex in the real atmosphere than in our model.

A different impression is gained from a recent study by Deser and Timlin (1997), who performed SVD analysis upon 14 years of weekly regional SST and $Z_{500\ mb}$ data, thus emphasizing shorter period fluctuations. Over both the Atlantic and Pacific the correlations between the atmospheric and oceanic components of the two leading SVD modes are strongest when the atmosphere leads by 2 or 3 weeks. The Atlantic SST patterns are very similar to those obtained using SST tendency, and the same is true over the Pacific when interannual fluctuations are filtered out. Furthermore, the spatial distribution and magnitude of these tendencies are in agreement with those implied by the concurrent surface heat flux anomalies. Thus, on seasonal and shorter timescales air–sea coupling is largely characterized by the atmosphere forcing the ocean.

The model's portrayal of the midlatitude coupled atmosphere–ocean as an essentially one-way forced system, in which the SST influence on the atmosphere is manifested as enhanced variance and persistence of the natural uncoupled variability but does not result in the direct generation of atmospheric perturbations, appears therefore to be relevant to the intraseasonal timescale at least. Indeed, the leading Atlantic SVD mode is remarkably similar to its observational analog in Deser and Timlin (1997), especially its western-Atlantic-like (WA) atmospheric component, which is associated with fluctuations in the index cycle (cf. our Fig. 12b with their Fig. 1c). The simulated 4-week SST response time is also in line with the observed 2–3-week lag. The observed leading SVD mode does not explain as overwhelming a fraction of the total squared covariance as in our model, but this is merely consistent with the fact that in the real world there are more degrees of freedom in the atmospheric circulation (i.e., there are flow patterns other than the WA pattern that are important in forcing the ocean).

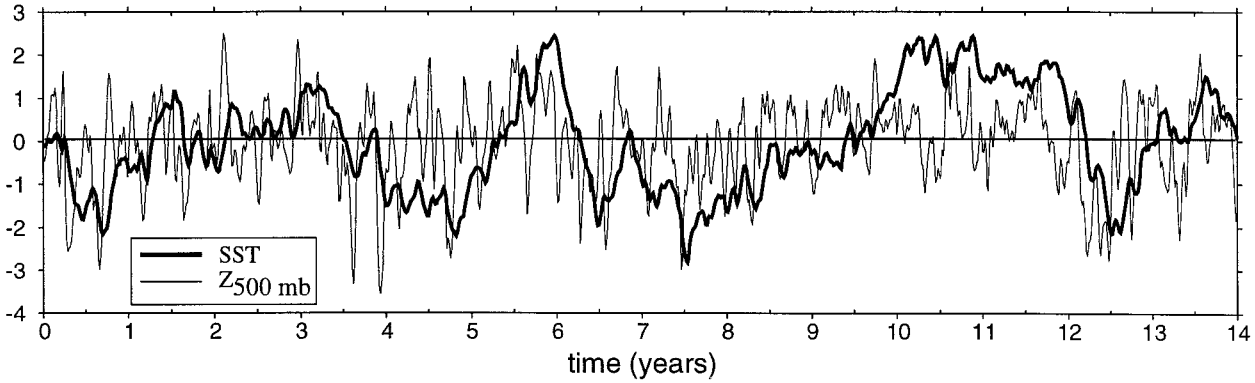

FIG. 15. Fourteen-year segment of the normalized expansion coefficient time series of the leading SVD mode of 500-mb geopotential height and Atlantic SST, computed using pentad data. The time series have been smoothed with a 1–2–1 filter. The correlation coefficient between the two time series is 0.54 when the SST lags by 30 days.

The main difference between our results and the observations is that the temporal relationship between the atmospheric and oceanic fields (i.e., the coupling) is weaker in our results: the maximum correlation for observed weekly averaged data is 0.69 but only 0.54 when the same filter used in Deser and Timlin (1997) is applied to our pentad model data. The reason for this can be understood by inspecting the time series of the 500-mb height and SST anomaly patterns associated with the leading Atlantic SVD mode of pentad data (Fig. 15) and comparing them with their observational analog (Deser and Timlin's Fig. 2). The local Atlantic zonal index mode exhibits a much higher level of random (high-frequency) variability in the simulation, to the point that the 1-month lag is barely visible. This may be due to the fact that the transient eddies in this coarse resolution model are not strong enough to lock the ''vacillation'' in one of its phases for long periods of time (Yu and Hartmann 1993). The SST, whose evolution can be viewed as a low-pass-filtered response to short timescale atmospheric forcing (Frankignoul and Hasselman 1977), is thus less well correlated with the geopotential height in the model than in the observations.

In the Pacific region the patterns associated with the simulated leading SVD mode and with the corresponding (intraseasonal) mode in Deser and Timlin (1997) do not match as closely as they do over the Atlantic, but the lead/lag relationships between the model atmospheric circulation and the SST field are again in qualitative agreement with the observations. In summary, the prevalent form of midlatitude atmosphere–ocean interaction that takes place in our atmospheric GCM with an embedded mixed layer is consistent with the observed spatial and temporal associations between the atmosphere and the extratropical oceans on seasonal and shorter timescales.

d. Atmospheric ''response'' versus natural uncoupled variability

Even though the higher-order modes account for only a very minor fraction of the total covariance it is worth examining them in some detail. It is conceivable that if atmosphere–ocean interactions exist in which the ocean plays more than a passive role, they would be associated with optimally located, small-scale SST anomalies whose contribution to the total covariability is small. This is suggested from fixed SST GCM experiments, which show that the atmosphere is most sensitive to localized SST forcing positioned in regions of maximum cyclogenesis (e.g., Ferranti et al. 1994).

The second SVD mode of 90-day mean Atlantic SST and $Z_{500\ mb}$, which explains 8.5% of the squared covariance, pairs the second EOF of SST in the Atlantic sector (Fig. 10b) with the pattern of height anomalies presented in Fig. 16, where the latter leads the former by one ''season.'' Once again, the SST pattern is consistent with direct forcing by the anomalous surface fluxes implied by the concurrent temperature and surface wind fluctuations (not shown). The pentad-data analysis indicates that the coupling is strongest when the atmosphere leads by 2 weeks. Analogous considerations apply to the second SVD mode over the Pacific sector (SCF = 11.6%, not shown).

The second Atlantic SVD mode is of particular interest because its oceanic pattern (Fig. 10b) bears some resemblance to the western Atlantic SST anomaly prescribed in the GCM experiments of Palmer and Sun (1985) and Peng et al. (1995), where it was shown to induce a significant atmospheric response. Additionally, the cross correlation for this SVD mode (Fig. 13b) does not drop to zero as fast as for the other modes but remains weakly positive at all lags. One may wonder whether this more symmetric lag-correlation function is not a reflection of a weak *dynamical* two-way atmosphere–ocean interaction in the manner discussed in section 5b, which would result in enhanced persistence of both atmospheric and oceanic anomalies. To ascertain the likelihood of this scenario and assess the potential impact of an SVD-2 (or EOF-2) SST anomaly on the atmospheric circulation, we constructed composite maps for extreme warm and cold episodes of this oceanic anomaly.

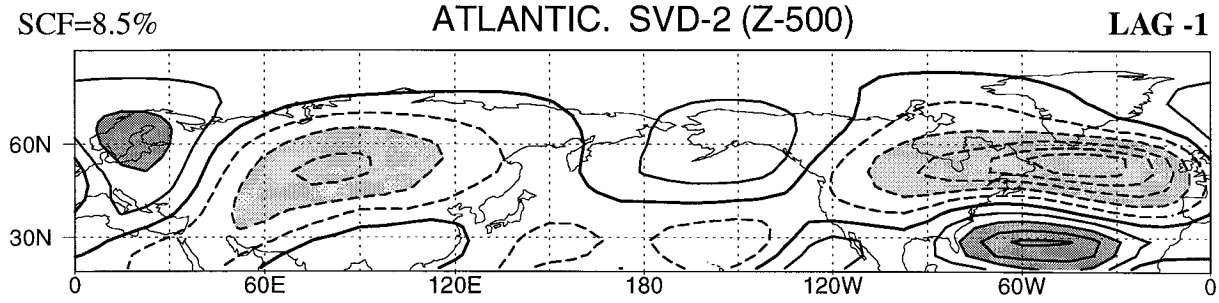

FIG. 16. The heterogeneous correlation pattern of 500-mb geopotential height for the second SVD mode of 90-day mean $Z_{500\,mb}$ and Atlantic SST for the atmosphere leading the ocean by 1 lag. The corresponding SST pattern is virtually identical to the second EOF of Atlantic SST (Fig. 10b) in the polarity shown. The contour interval is 0.1; the thick line is the zero contour. Dark (light) shading indicates correlations larger (smaller) than 0.1 (-0.1). The correlation between atmospheric and oceanic anomalies is 0.64 at this lag.

Monthly time series of EOF-2 of Atlantic SST were used for our purpose. *Individual* warm and cold SST events were selected by requiring that each event be separated from the previous one by 4 months or more. The month chosen to enter the composite as month 0 corresponds to the first month in a given period to exceed the selected threshold (this turns out to be the peak time of the composite SST anomaly). The threshold was chosen so that 20 events could be found to form each composite (around ± 1.2 K). The time evolution of the $Z_{500\,mb}$ anomaly composites from month -1 to month $+3$ for the warm and cold episodes is presented in Fig. 17, together with the corresponding SST composite on month 0. Regions where the composites are statistically significant at the 90%, 95%, and 99% levels (assuming 19 degrees of freedom and a two-sided Student's *t*-distribution) are colored in different shades of gray.

Persistent large-scale SST anomalies with maximum amplitude around 1.7 K are observed during these periods. The most striking feature of the $Z_{500\,mb}$ composites is that the anomalies at month $+2$ for both warm and cold events are much more significant than on the month following the peak time of the SST anomalies ($+1$) and at least as significant as the simultaneous anomalies. The strongest pattern is of course found on the preceding month (-1) and its structure is that anticipated from the SVD analysis (Fig. 16). It weakens considerably over the next month and has completely disappeared by month $+1$. On month $+2$ a new dipolar atmospheric perturbation whose centers of action are significant at the 99% level emerges over the *same* region in both composite series (it is therefore valid to use a priori confidence limits). This dipole is also evident at the surface (not shown) and straddles the SST anomaly, with a node around 50°N.

Oddly though, this dipole exhibits the *same* polarity for both warm and cold events, with a large anticyclone north of the SST extremum. Moreover, notice that what one might be tempted to call the atmospheric ''response'' to the SST anomaly bears a strong resemblance to the leading mode of low-frequency variability in its local Atlantic manifestation (recall Figs. 3a and 12). Composites of the projection of the $Z_{500\,mb}$ field on this EOF-1 reveal that on month $+2$ the projection is significant at the 95% level for both warm and cold events (Fig. 18). It is, however, also clear from this figure that projections of this size are not unusual for what amounts to be a randomly chosen group of months (e.g., month -5, *before* the advent of the SST anomaly).

In the presence of such a lively mode of variability it becomes difficult to assess the degree to which the statistically significant height anomalies that appear around month $+2$ following an Atlantic EOF-2 SST event are truly different from the *natural uncoupled* variability of the atmosphere. A comparison of the ''coupled'' evolution of the geopotential height pattern associated with the SVD-2 mode (as seen in Fig. 17) with its uncoupled life cycle in the control experiment serves only to complicate matters. We find that, in a statistical sense, a typical ''uncoupled'' $Z_{500\,mb}$ anomaly like that on month -1 also develops into a significant EOF-1-like perturbations with an anticyclone over Greenland, on the following month (not shown). We interpret this result as yet further evidence of the high degree of random variability of EOF-1.

In light of the similarity between the coupled and uncoupled behaviors we are skeptical that one can rightfully interpret the atmospheric anomalies on month $+2$ in Fig. 17 as a response to Atlantic SST anomalies. Moreover, one would still have to explain why such a response should be nonlinear. The possibility of a chance result is compounded by the fact that of all the SST anomalies examined (those corresponding to the four leading EOFs in each ocean and a few others taken from observational and modeling studies), this was the only one that was associated with significant atmospheric anomalies on the following months.

6. Conclusions and discussion

a. Summary

This study has expanded upon the results of Barsugli (1995) and Delworth (1996) to present a comprehensive picture of how the intrinsic midlatitude low-frequency

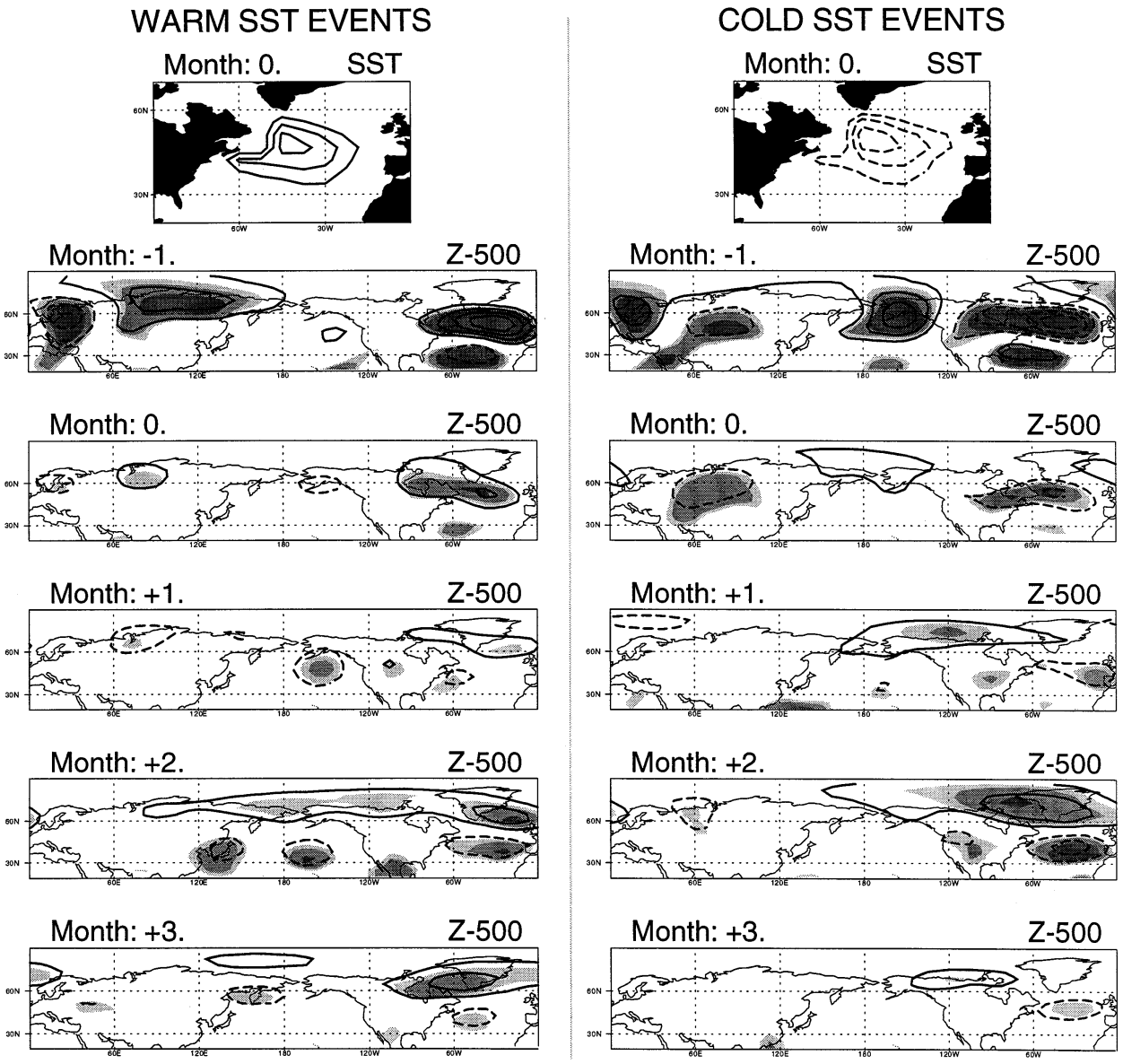

FIG. 17. Composite maps of monthly mean SST and 500-mb geopotential height for 20 extreme warm and cold events of EOF 2 of Atlantic SST. Left panels: warm events; right panels: cold events. The top panel shows the SST anomaly composite on month 0; contour interval is 0.5 K. The remaining panels show the composite 500-mb height anomalies on months −1 to +3; contour interval is 20 m. The three grades of shading indicate a priori statistical significance at the 90% (lighter), 95%, and 99% (darkest) levels. The zero contour has been omitted on all plots.

atmospheric variability in a realistic GCM is altered by the presence of an inert, constant-depth oceanic mixed layer. Another goal was to document the temporal and spatial characteristics of the dominant patterns of covariability between the hemispheric circulation and the extratropical SST in the absence of explicit interannual variability.

We find that the interaction with the mixed layer does not substantially modify the variance of midtropospheric geopotential height, nor does it affect the spatial organization of the variability: coupling reddens the spectrum of 500-mb height without transforming the existing, or generating new, anomaly patterns. The variance associated with the leading mode of low-frequency variability—a zonally symmetric dipolar pattern with maximum amplitude over the oceans—is preferentially enhanced by the coupling. The second mode (another large-scale structure) is also affected but to a much lesser extent.

As in Barsugli's idealized two-level model coupling significantly enhances the variance of the lower-tropospheric thermal field. Because this effect mainly involves the *adjustment* of the mixed layer to overlying atmospheric perturbations on timescales longer than the decorrelation time of the mixed layer (Barsugli 1995),

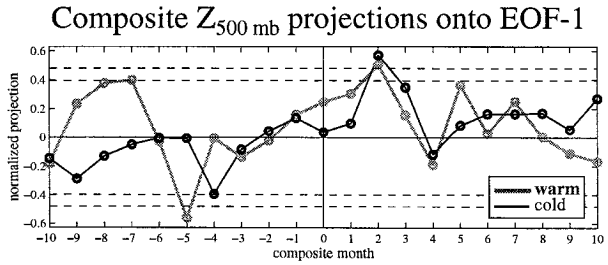

FIG. 18. Composite normalized projection of monthly mean 500-mb geopotential height anomalies onto the leading EOF of this field (Fig. 3) relative to 20 warm (gray line) and cold (black line) events of EOF 2 of Atlantic SST. The corresponding composite patterns of $Z_{500\,mb}$ on months -1 to 3 are those shown in Fig. 17. The dashed lines indicate the value at which the projection becomes statistically significant at the 90% and 95% levels.

this increase is felt mostly locally and at annual or lower frequencies. In the uncoupled (fixed SST) case surface heat fluxes essentially act to damp surface air temperature variations. Coupling enhances the low-frequency thermal variance, and hence the persistence of atmospheric circulation anomalies, by reducing this negative *thermal* feedback associated with surface heat fluxes, and not by directly generating atmospheric anomalies.

Though the SST variability is too weak compared to observations, the preferred oceanic patterns have large spatial scales and their general structure resembles the observations, particularly over the Atlantic. The dominant SVD mode of 90-day mean or pentad-mean hemispheric circulation ($Z_{500\,mb}$) and Atlantic or Pacific SST pairs the leading EOF in each ocean with the dominant mode of natural *uncoupled* atmospheric variability. Identical results are obtained using SST tendency. The fine-resolution analysis indicates that the ocean is lagging the atmosphere by about 4 weeks. The SST structures are consistent with direct forcing by the anomalous heat fluxes implied by the attendant surface air temperature and wind fluctuations, as deduced from analogous SVD expansions using SLP and $T_{850\,mb}$ as the atmospheric variable. The very asymmetric nature of the cross-correlation function about zero lag confirms our earlier impression that large-scale air–sea interaction in the model is largely characterized by one-way atmospheric forcing of the mixed layer, with little or no *dynamical* feedback in the other direction. The mixed layer does more than passively respond to the atmosphere, since it acts to slightly extend the lifetime of the atmospheric anomalies, but it does not play a role in the temporal evolution of the coupled system from one regime to another, or in the spatial organization of the covariability; these are entirely controlled by the atmosphere.

Lastly, composite analyses based on *extreme* SST anomaly events reveal no evidence of direct forcing of atmospheric perturbations by SST anomalies. Composites for extreme episodes of EOF 2 of Atlantic SST (a monopolar anomaly south of Greenland) suggest that a statistically significant atmospheric perturbation develops following the peak time of the SST anomaly. This perturbation, however, projects strongly onto the leading mode of natural uncoupled variability—a mode that is conspicuously present throughout the integration—and does not appear to be a ''response'' to the SST anomaly.

b. Discussion

Based on observations alone it is impossible to ascertain whether, despite the asymmetric correlations suggesting atmospheric forcing of the SST anomalies, the midlatitude oceans are involved or not in establishing the observed dominant patterns of atmospheric circulation. Inasmuch as the GCM mimics the real situation, we can assert the answer is no. On the other hand, we can corroborate Barsugli's (1995) result that coupling leads to qualitative changes in the low-frequency variability, in the form of enhanced thermal variance and persistence of certain atmospheric structures for which the interaction with the mixed layer preferentially reduces the damping.

The exact form and efficiency of this ''selective enhancement'' mechanism will depend on the details of the model and the nature of the uncoupled low-frequency variability. In Barsugli's all-ocean model, these ''least damped'' modes are selected based on their large zonal scale and low phase speed. In a geographically realistic model, those structures that, in addition, have maximum amplitude and maximum area coverage over the ocean will clearly be favored over the others, hence the preferential amplification of the leading mode—though other factors are probably important in singling out this mode. Lack of geopotential height data at levels other than 500 mb has prevented us from examining the relation between the vertical structure of a mode and the efficiency of coupling for this mode. The vertical distribution of the diabatic heating associated with surface fluxes must also play a role. One may think of this ''selective enhancement'' as a form of weak resonance (J. Barsugli 1996, personal communication).

Increased low-level thermal variance and reduced surface fluxes at low frequencies as a result of coupling have also been reported in studies involving more realistic ocean models and a seasonal cycle (Manabe and Stouffer 1996; U. S. Bhatt et al. 1997, manuscript submitted to *J. Climate*). The robustness of these results suggests that they might be viewed as representing the baseline (or zeroth order) effect of midlatitude coupling, irrespective of any unstable air–sea interactions that might develop in a more sophisticated coupled model or in the real world. This generic behavior can also be qualitatively reproduced in a one-dimensional stochastically forced linear coupled model (Barsugli and Battisti 1997).

The simple coupling dynamics at work in this GCM with an embedded motionless mixed layer in midlatitudes and no interannual tropical SST forcing are able to capture the essential nature of the observed extratropical

atmosphere–ocean interaction on weekly-to-seasonal timescales, as documented in Deser and Timlin (1997). Over the Atlantic, model and observations agree with respect to the spatial structure of the coupling: the dominant mode of covariability is characterized by the local manifestation of the index cycle (WA-like pattern) leading a collocated ''sandwich''-like pattern in the ocean (EOF-1 of Atlantic SST). Over the Pacific, which is under the influence of ENSO and exhibits a larger proportion of interannual variability, the spatial similarities between the simulated and observed patterns are less remarkable. The main difference with observations is the lower temporal correlation between oceanic and atmospheric components (i.e., weaker coupling) and the excessive dominance of this mode of interaction. Both of these are related to inadequacies in the simulation of the zonally symmetric low-frequency atmospheric variability and are probably due to insufficient model resolution. Overall, though, our results support the notion that on intraseasonal timescales, at least, the atmosphere is driving the ocean.

Extratropical air–sea interaction may take on different characteristics on longer interannual timescales. In contrast with analysis of covariability using SST tendency or a dataset that emphasizes short-term fluctuations (Wallace et al. 1990; Deser and Timlin 1997), those based on seasonal means and longer records reveal altogether different patterns of more global extent (Wallace et al. 1990, 1992). Nevertheless, we will show in Part II that when interannual variability is introduced in the model via remote tropical Pacific SST forcing, the patterns of midlatitude covariability possess the same kind of intraseasonal/interannual duality exhibited by the observations, but the basic conclusions from this study are unaltered.

We find no indication that SST anomalies are capable of directly forcing atmospheric perturbations. These conclusions may be marred by the fact that low-resolution models, and this GCM in particular, are renowned for being rather insensitive to lower boundary forcing (see Kushnir and Held 1996), presumably because of their inability to properly resolve the effects of synoptic eddies in the stormtracks. Indeed the high-resolution GCM experiments of Palmer and Sun (1985), Ferranti et al. (1994), and Peng et al. (1995) suggest that the atmosphere is able to react to certain fixed SST anomalies; their diagnostic analyses indicate that transient eddy transports may be instrumental in eliciting and maintaining a response. The imposed SST anomalies are also significantly larger than what this model is capable of generating (indeed, unrealistically large). Another important factor appears to be the basic state, with a perpetual November atmosphere exhibiting a much higher sensitivity to SST forcing than a perpetual January one (Peng et al. 1995; Y. Kushnir 1996, personal communication).

However, one should not infer from these studies that under similar conditions a *coupled* model atmosphere will be equally perturbed by SST anomalies that it generated in the first place, since the mutual adjustment of the ocean and atmosphere is likely to result in a qualitatively different behavior. The results from this study confirm Barsugli's (1995) impression that the influence of SST anomalies manifests itself as a ''reorganization'' of the natural uncoupled variability, rather than as an atmospheric ''response.'' The distinction is more than a semantic one. We believe that *SST anomalies in the real world act to bias the atmospheric circulation toward certain flow regimes by increasing their persistence.* This effect simply results from the large heat capacity of the mixed layer, which constrains the atmospheric anomalies to stay in place for longer than they would on their own. One may think of the overall effect of coupling as *inducing a slight shift in the probability density distribution of atmospheric states.* These ideas echo those expressed by Palmer (1995), who views the role of SST anomalies in climate as qualitatively equivalent to a ''storage'' or ''capacitor'' device. Palmer also discusses the potential grim implications for predictability. If indeed the source of the variability resides in the atmosphere, the predictability of the coupled system cannot benefit much from this added storage term.

It is possible that these reorganization dynamics may take on a different form if the atmosphere is coupled to a full dynamical ocean model capable of generating its own SST anomalies, but even that does not guarantee a coupled behavior that is analogous to the direct one-way forcing scenario illustrated by prescribed SST experiments. The order of magnitude difference between the coupled atmospheric anomaly associated with Latif and Barnett's (1994) interdecadal mode and the direct response of their model atmosphere to the corresponding SST anomaly is a good reminder of such distinction. Recall, also, that Delworth's (1996) and Manabe and Stouffer's (1996) results from their full-ocean coupled experiment did not differ significantly from their mixed-layer results, although, since the atmospheric component was the same low-resolution model used here, their conclusions are to be taken with some caution.

As was shown in the last section, in a coupled simulation the presence of a statistically significant signal following the advent of an SST anomaly does not guarantee a ''response.'' This example illustrates the fact that one must be very careful when assessing the SST influence on the atmospheric circulation and should serve as a warning for future diagnoses of atmospheric ''responses'' in high-resolution coupled GCM experiments with full dynamical oceans. These, undoubtedly, hold the key to future progress on the issue of extratropical air–sea interactions. We believe that a consistent approach would be to perform long *coupled* simulations in conjunction with *fixed* SST simulations, using the SST anomalies that the coupled model can internally generate. Only then will we be able to reconcile the results from coupled and one-way forcing experiments and achieve a unified understanding of the midlatitude atmosphere–ocean coupled system.

Acknowledgments. I would like to thank Professor Mike Wallace for his valuable comments and suggestions throughout the course of this study. Discussions with Joe Barsugli and Nate Mantua and comments by David Battisti, Tim Palmer, and Mike Alexander greatly improved the original manuscript. Gregor Nitsche unpacked the data and kindly shared some of his code with me. This research was supported by NOAA under Cooperative Agreement NA37RJ0198.

REFERENCES

Barnett, T. P., 1981: Statistical prediction of North American air temperature from Pacific predictors. *Mon. Wea. Rev.,* **109,** 1021–1041.

——, and R. C. J. Somerville, 1983: Advances in short-term climate prediction. *Rev. Geophys.,* **21,** 1096–1102.

Barsugli, J. J., 1995: Idealized models of intrinsic midlatitude atmosphere–ocean interaction. Ph.D. dissertation, University of Washington, 187 pp. [Available from University of Washington, Dept. of Atmospheric Sciences, Box 351640, Seattle, WA 98195-1640; or on-line from http://www.cdc.noaa.gov/~jjb/thesis.html.]

——, and D. S. Battisti, 1997: The basic effects of atmosphere–ocean thermal coupling on midlatitude variability. *J. Atmos. Sci.,* in press.

Battisti, D. S., U. Bhatt, and M. A. Alexander, 1995: A modeling study of the interannual variability in the wintertime North Atlantic Ocean. *J. Climate,* **8,** 3067–3083.

Cayan, D., 1992: Latent and sensible heat flux anomalies over the northern oceans: Driving the sea surface temperature. *J. Phys. Oceanogr.,* **22,** 859–881.

Davis, R. E., 1978: Predictability of sea level pressure anomalies over the North Pacific Ocean. *J. Phys. Oceanogr.,* **8,** 233–246.

Delworth, T. L., 1996: North Atlantic interannual variability in a coupled ocean–atmosphere model. *J. Climate,* **9,** 2356–2375.

Deser, C., and M. L. Blackmon, 1995: On the relationship between tropical and North Pacific sea surface temperature variations. *J. Climate,* **8,** 1677–1680.

——, and M. S. Timlin, 1997: Atmosphere–ocean interaction on weekly timescales in the North Atlantic and Pacific. *J. Climate,* **10,** 393–408.

Ferranti, L., F. Molteni, and T. N. Palmer, 1994: Impact of localized tropical and extratropical SST anomalies in ensembles of seasonal GCM integrations. *Quart. J. Roy. Meteor. Soc.,* **120,** 1613–1645.

Frankignoul, C., 1985: Sea surface temperature anomalies, planetary waves and air-sea feedback in the middle latitudes. *Rev. Geophys.,* **23,** 357–390.

——, and K. Hasselmann, 1977: Stochastic climate models, II. Application to sea-surface temperature variability and thermocline variability. *Tellus,* **29,** 284–305.

——, and R. W. Reynolds, 1983: Testing a dynamical model for midlatitude sea surface temperature anomalies. *J. Phys. Oceanogr.,* **13,** 1131–1145.

Gallimore, R. G., 1995: Simulated ocean–atmosphere interaction in the North Pacific from a CGM coupled to a constant-depth mixed layer. *J. Climate,* **8,** 1721–1737.

Haney, R. L., 1985: Midlatitude sea surface temperature anomalies: A numerical hindcast. *J. Phys. Oceanogr.,* **15,** 787–799.

Karoly, D. J., 1990: The role of transient eddies in low-frequency zonal variations in the Southern Hemisphere circulation. *Tellus,* **42A,** 41–50.

Kushnir, Y., and I. M. Held, 1996: Equilibrium atmospheric responses to North Atlantic SST anomalies. *J. Climate,* **9,** 1208–1220.

Latif, M., and T. P. Barnett, 1994: Causes of decadal climate variability over the North Pacific and North America. *Science,* **266,** 634–637.

Lau, N.-C., 1985: Modeling the seasonal dependence of the atmospheric response to observed El Niños in 1962–76. *Mon. Wea. Rev.,* **113,** 1970–1996.

——, and M. J. Nath, 1990: A general circulation model study of the atmospheric response to extratropical SST anomalies observed in 1950–1970. *J. Climate,* **3,** 965–989.

——, and ——, 1996: The role of the ''atmospheric bridge'' in linking tropical Pacific ENSO events to extratropical SST anomalies. *J. Climate,* **9,** 2036–2057.

Manabe, S., and R. J. Stouffer, 1996: Low-frequency variability of surface air temperature in a 1000-year integration of a coupled atmosphere–ocean–land surface model. *J. Climate,* **9,** 376–393.

Namias, J., 1950: The index cycle and its role in the general circulation. *J. Meteor.,* **7,** 130–139.

——, 1973: Thermal communication between the sea surface temperature and the lower troposphere. *J. Phys. Oceanogr.,* **3,** 373–378.

Newman, M., and P. D. Sardeshmukh, 1995: A caveat concerning singular value decomposition. *J. Climate,* **8,** 352–360.

Nitsche, G., 1996: Some aspects of planetary-scale atmospheric variability in a low-resolution general circulation model. Ph.D. dissertation, University of Washington, 207 pp. [Available from University of Washington, Dept. of Atmospheric Sciences, Box 351640, Seattle, WA 98195-1640.]

North, G. R., T. L. Bell, R. F. Cahalan, and F. J. Moeng, 1982: Sampling errors in the estimation of empirical orthogonal functions. *Mon Wea. Rev.* **110,** 699–706.

Palmer, T. N., 1995: The influence of north-west Atlantic sea surface temperature: An unplanned experiment. *Weather,* **50,** 413–419.

——, and Z. Sun, 1985: A modelling and observational study of the relationship between sea surface temperature in the northwest Atlantic and the atmospheric general circulation. *Quart. J. Roy. Meteor. Soc.,* **111,** 947–975.

Peng, S., and J. Fyfe, 1996: The coupled patterns between sea level pressure and sea surface temperature in the midlatitude North Atlantic. *J. Climate,* **9,** 1824–1839.

——, L. A. Mysak, H. Ritchie, J. Derome, and B. Dugas, 1995: The differences between early and midwinter atmospheric responses to sea surface temperature anomalies in the northwest Atlantic. *J. Climate,* **8,** 137–157.

Robinson, W. A., 1991: The dynamics of the zonal index in a simple model of the atmosphere. *Tellus,* **43A,** 295–305.

Rossby, C.-G., and Coauthors, 1939: Relation between variations in the intensity of the zonal circulation of the atmosphere and the displacements of the semi-permanent centers of action. *J. Mar. Res.,* **2,** 38–55.

Wallace, J. M., and D. S. Gutzler, 1981: Teleconnections in the geopotential height field during the Northern Hemisphere winter. *Mon. Wea. Rev.,* **109,** 784–812.

——, C. Smith, and Q. Jiang, 1990: Spatial patterns of atmosphere–ocean interaction in the northern winter. *J. Climate,* **3,** 990–998.

——, and C. S. Bretherton, 1992: Singular value decomposition of wintertime sea surface temperatures and 500-mb height anomalies. *J. Climate,* **5,** 561–576.

Wetherald, R. T., and S. Manabe, 1988: Cloud feedback processes in a general circulation model. *J. Atmos. Sci.,* **45,** 1397–1415.

Yu, J.-Y., and D. L. Hartmann, 1993: Zonal flow vacillation and eddy forcing in a simple GCM of the atmosphere. *J. Atmos. Sci.,* **50,** 3244–3259.